




Cite this: *Energy Environ. Sci.*,
2019, 12, 492

Pt-Based electrocatalysts with high atom utilization efficiency: from nanostructures to single atoms

Lei Zhang, Kieran Doyle-Davis and Xueliang Sun *

In recent years, development to increase the performance of Pt-based catalysts and reduce the cost has received significant attention. Among them, the preparation of Pt-based catalysts with high atom utilization efficiency can induce more active sites between the Pt atoms and participating molecules, resulting in improved mass activity. In addition, the combination of high atom utilization efficiency with well-controlled surface structure and composition could boost the mass activity for Pt-based catalysts. This review describes recent progress in the design and synthesis of Pt-based catalysts with high atom utilization efficiency and their enhanced catalytic performance in electrochemical catalytic reactions. The significance for the fabrication of nanostructures and single atom catalysts with high atom utilization will be presented in the introduction section. We discuss the synthetic strategies according to two routes: (1) the rational design of Pt nanostructures, including porous, nanowire, core-shell and hollow structures; and (2) preparation of Pt single atom catalysts and the stabilization of single atoms. Additionally, we discuss the superior electro-catalytic applications of Pt-based catalysts with high atom utilization efficiency. These recent advancements in rational design of Pt-based catalysts offer numerous cases for potential industrialized catalysts with high mass activity and reduced cost in the future.

Received 5th October 2018,
Accepted 6th December 2018

DOI: 10.1039/c8ee02939c

rsc.li/ees

Broader context

Pt-Based catalysts have attracted increased attention due to their unique electrochemical catalytic properties, involving the oxygen reduction reaction, hydrogen evolution reaction *etc.* Notwithstanding the superior properties of Pt catalysts, the low abundance of Pt and subsequent high cost hinder the commercial application of Pt catalysts. With the development of heterogeneous catalysis, surface science and nanotechnology, it has been extensively proved that the improvement of the atom utilization efficiency (AUE) of Pt catalysts can effectively reduce catalyst cost and simultaneously improve their electrochemical properties. To achieve a high AUE of Pt, Pt nanocrystals were rationally designed as some specific structures (such as porous, nanowire, core-shell and hollow structures). Additionally, a maximum efficiency of 100% can be reached when the size of Pt catalysts is reduced to single atoms. This review focused on synthetic strategies of high AUE Pt-based catalysts from nanostructures to single atoms. The rational design of Pt-based catalysts with high AUE will lead to new highly active Pt catalysts for electrochemical reactions. Additionally, the systematic synthesis of Pt catalysts would provide useful experience for preparation of other noble metal catalysts.

1. Introduction

Noble metal nanocatalysts are widely seen in several industrial applications due to their unique intrinsic properties and catalytic activities. Pt, as one typical noble metal, has received increased attention due to its irreplaceable catalytic properties in many areas, including the energy, pharmaceutical, petroleum, and automotive industries.^{1–4} In recent years, Pt has been considered to be an effective catalyst in fuel cell-related reactions. Pt-Based catalysts exhibit great electrochemical performance in both anode and

cathode catalytic reactions.^{5–8} At this point, several types of fuel cells have achieved being commercialized. For example, the Toyota Mirai, which is equipped with a proton exchange membrane fuel cell, was unveiled at the November 2014 Los Angeles auto show.⁹ Direct methanol fuel cells and direct formic acid fuel cells can produce a small amount of power over a long period, ideal for mobile phones and other portable electronics.^{10–13} Notwithstanding the superior properties of Pt catalysts, the low abundance of Pt and subsequent high cost hinder the commercial application of Pt catalysts.

With the development of heterogeneous catalysis, surface science and nanotechnology, it has been extensively proved that the properties of Pt catalysts are highly dependent on their

Department of Mechanical and Materials Engineering, The University of Western Ontario, London, ON N6A 5B9, Canada. E-mail: xsun@eng.uwo.ca

composition, atom arrangement on surfaces and surface area.^{14–19} With the fabrication of bimetallic or trimetallic catalysts, the performance can be improved due to ensemble and ligand effects. For example, with the formation of a PtNi bimetallic structure, the oxygen reduction reaction (ORR) properties can be significantly improved compared with pure Pt catalysts.^{20–26} However, the alloy structure is not stable during the ORR test, and Ni atoms tend to be corroded during the reaction. As a result, the alloy structures can not maintain good stability during long-term testing. Another route for enhancing the electrochemical activity is to design the surface structure of Pt-based catalysts. With the understanding of growth theories of nanocrystals, Pt catalysts with different surface arrangements have been successfully prepared. Pt catalysts with

high-index facets exhibited greatly enhanced activity towards formic acid oxidation.^{27–32} It should be pointed out that most of the well-controlled Pt catalysts have a large particle size, which induces a smaller surface area. Accordingly, most of the catalysts exhibit good specific activity normalized by the electrochemically active surface area (ECSA); yet their mass activity was not obviously improved. Among various different routes for improving the activity of Pt catalysts, one of the most direct routes to increase mass activity for Pt catalysts is to increase the atom utilization efficiency (AUE) by designing some specific structures (such as porous, nanowire, core-shell and hollow structures) or reducing the particle size to single atom catalysts. The AUE is the ratio of atoms exposed on the surface to the total atoms in the catalysts. The AUE can be increased by reducing the particle size, thus providing more active sites between the Pt atoms and participating molecules. For example, the AUE of Pt atoms can be increased from 9.5% to 26% by reducing the edge length of a Pt cube from 11.7 to 3.9 nm. However, Pt catalysts with extremely small size tend to sinter (form larger particles) and detach from the support during operation.

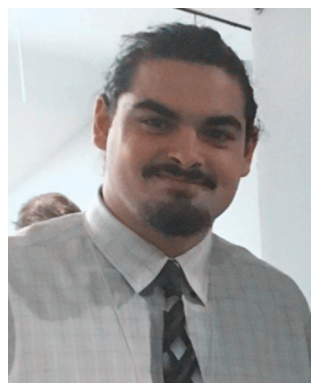
Consequently, it is of great importance to develop synthetic strategies for Pt based catalysts with high AUE. In recent years, significant progress has been made on this point and several different types of nanostructures and Pt-based single atom catalysts have been successfully synthesized. However, most reviews have focused on a summary of the composition or shape-controlled synthesis of Pt-based catalysts. Few discussions on the AUE of Pt catalysts can be found in recent reviews. As such, a comprehensive and inspiring summary of Pt-based nanocrystals with extremely high AUE for catalytic applications is meaningful to present. This review describes recent progress on the syntheses, characterization and catalytic applications of Pt based catalysts with high AUE. The summary of improvement of AUE is described through two routes: (1) the rational design of Pt nanostructures; and (2) the preparation of Pt single atom catalysts. In regards to



Lei Zhang

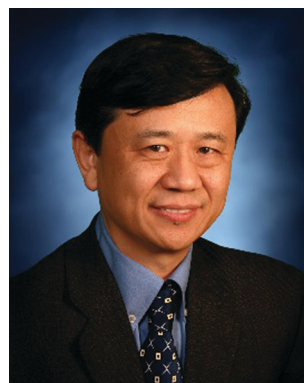
Lei Zhang received his BS degree in Chemistry (2008) and PhD degree in Nanomaterial Chemistry (2014) from Xiamen University with Prof. Zhaoxiong Xie. He was a visiting graduate student at Georgia Institute of Technology in Prof. Younan Xia's group from 2012 to 2014. From 2015 to 2016, he worked as a Postdoc at Collaborative Innovation Center of Chemical Science and Engineering at Tianjin University. He is currently a postdoctoral associate with Professor Xueliang Sun at University of Western Ontario. His research interests include the design and synthesis of metal nanomaterials and single atom catalysts for fuel cells, carbon dioxide reduction, and water splitting devices.

Lei Zhang received his BS degree in Chemistry (2008) and PhD degree in Nanomaterial Chemistry (2014) from Xiamen University with Prof. Zhaoxiong Xie. He was a visiting graduate student at Georgia Institute of Technology in Prof. Younan Xia's group from 2012 to 2014. From 2015 to 2016, he worked as a Postdoc at Collaborative Innovation Center of Chemical Science and Engineering at Tianjin University. He is currently a postdoctoral associate with Professor Xueliang Sun at University of Western Ontario. His research interests include the design and synthesis of metal nanomaterials and single atom catalysts for fuel cells, carbon dioxide reduction, and water splitting devices.



Kieran Doyle-Davis

Kieran Doyle-Davis received his Honours BSc in Physics from McMaster University in 2018, with research focus on process optimization for lithium ion battery fabrication, and thin polymer films. Kieran is currently an MESC candidate at the University of Western Ontario under the supervision of Prof. Xueliang Sun. His current research interests include the development of next generation surface modified 3-D current collectors for both solution and solid-state lithium ion batteries.



Xueliang Sun

Prof. Xueliang (Andy) Sun is a Canada Research Chair in Development of Nanomaterials for Clean Energy, Fellow of the Royal Society of Canada and Canadian Academy of Engineering and Full Professor at the University of Western Ontario, Canada. Dr Sun received his PhD in materials chemistry in 1999 from the University of Manchester, UK, which he followed up by working as a postdoctoral fellow at the University of British Columbia, Canada and as a Research Associate at L'Institut National de la Recherche Scientifique (INRS), Canada. His current research interests are focused on advanced materials for electrochemical energy storage and conversion, including electrocatalysis in fuel cells and electrodes in lithium-ion batteries and metal-air batteries.

the rational design of Pt structures, we discuss four typical structures to improve; these are porous structures, ultrathin nanowires, core-shell nanoparticles with ultra-thin shells and nanocages with subnanometer walls. We will also discuss a number of synthetic strategies for controlling Pt single atom catalysts and improving the stability of single atom catalysts and clusters. Furthermore, we highlight several important electrocatalytic applications and enhanced mechanisms of Pt based catalysts with high AUE, including the ORR, methanol/formic acid oxidation reaction and hydrogen evolution reaction (HER).

2. Rational design of Pt nanostructures

2.1 Pt-Based porous structures

2.1.1 Hard template and soft template replication methods.

Due to the high surface energy of small clusters, Pt particles tend to sinter and aggregate during the catalytic reaction. For this reason, Pt-based porous structures are fabricated both to avoid aggregation and provide a high AUE. The interior atoms of the porous structures can take part in the reactions due to the channels on the surface. To fabricate porous Pt nanostructures, hard template and soft template replication methods are considered two effective protocols. For the hard template process, three main steps are involved to create Pt porous structures: (1) the preparation of a sacrificial template (silica, polymer, *etc.*), (2) deposition of Pt in the pores, and (3) removal of the template.³³ Based on this protocol, Kuroda and co-workers fabricated a dual template composed of assembled silica arrays and a Pluronic P123 block copolymer to synthesize cage-type mesoporous Pt nanostructures with adjustable large mesopores and rough surfaces.³⁴ Yamauchi *et al.* obtained olive-shaped mesoporous Pt nanoparticles by reducing Pt sources in a mesoporous silica (SBA-15) template (Fig. 1A and B).³⁵ Then, Yamauchi extended the hard template method to prepare mesoporous Pt-Ru alloy particles. Mesoporous Pt-Ru alloy particles with a pore size of 3.0 nm were obtained by using mesoporous silica as the template.³⁶

Soft template replication is another route to prepare Pt mesoporous structures. Lyotropic liquid crystals (LLCs), made of highly concentrated surfactants, possess long-range periodic nanostructures in the mesoscale range, which make them good soft templates for the preparation of mesoporous materials. In 1997, Attard and coworkers fabricated mesoporous Pt NPs from LLCs for the first time.³⁷ Yamauchi and co-workers found that the pore size of the obtained Pt mesoporous structure can be rationally designed by using LLCs composed of diblock copolymers. Mesoporous Pt particles with giant mesocages (approximately 15 nm) were synthesized *via* electrochemical deposition (Fig. 1C and D).³⁸ Another approach using soft templates is to use a micelle assembly in a low-concentration surfactant solution. In this procedure, surfactant micelles can form when the surfactant concentrations were set above the critical micelle concentration (CMC). Mesoporous Pt films with a wide range of controlled mesopore sizes can be constructed by using different surfactants and added organic expanders through potentiostatic deposition.³⁹

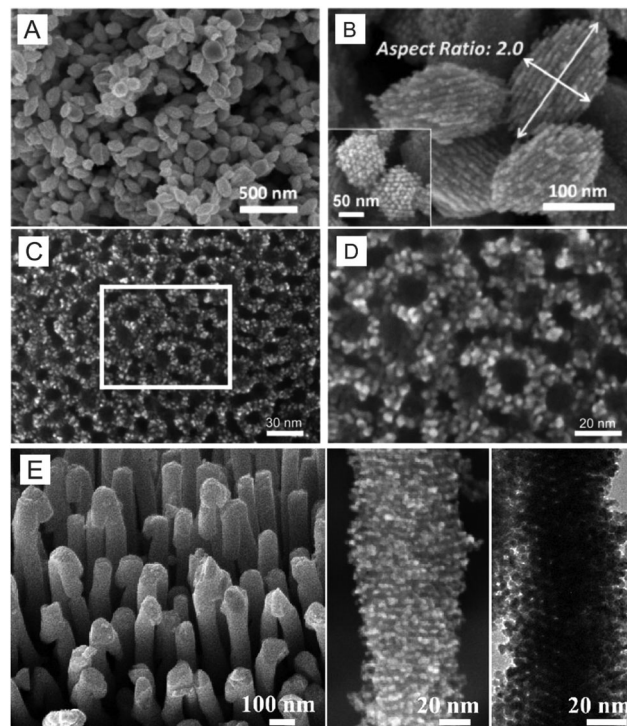


Fig. 1 (A and B) Scanning Electron Microscope (SEM) images of the mesoporous Pt particles prepared from mesoporous silica (SBA-15). Adapted with permission from ref. 35. Copyright 2012 Wiley-VCH. (C and D) SEM images of the mesoporous Pt particles prepared by using LLCs composed of diblock copolymers as the soft template. Adapted with permission from ref. 38. Copyright 2008 Wiley-VCH. (E) SEM and transmission electron microscope (TEM) images of the Pt fibers prepared from the LLCs and PAAMs. Adapted with permission from ref. 43. Copyright 2008 American Chemical Society.

In addition, bimetallic mesoporous films (Pt-Au, Pt-Ru and Pt-Pd) with tuneable composition can be obtained in the presence of different precursors.^{40–42} Furthermore, the hard template and soft template methods can be combined in one reaction system. Yamauchi prepared Pt mesoporous fibers by a dual-template route, which used LLCs as mesostructural direct templates and porous anodic alumina membranes (PAAMs) as morphological direct templates (Fig. 1E).⁴³

2.1.2 Highly branched Pt nanostructures. In recent years, highly branched Pt nanostructures have received a tremendous amount of attention due to their large surface area, high density of edge/corner atoms and tunable composition.^{44–57} Shelnutt *et al.* first reported the fabrication of Pt dendrites through an aqueous reduction method.⁴⁶ The uniform Pt dendrites can be prepared by using sodium dodecyl sulfate or polyoxyethylene (23) lauryl ether (Brij-35) as the surfactant and ascorbic acid as the reducing agent. Yamauchi prepared dendritic Pt nanoparticles by using the Pluronic F127 block copolymer (PEO₁₀₀PPO₆₅PEO₁₀₀) as the surfactant.⁴⁷ The Pluronic chains, which adsorbed on the Pt surface during the Pt deposition in this system, could form cavities and then facilitate the formation of the porous structure. The as-prepared dendritic Pt nanoparticles had a surface area of 56 m² g⁻¹, much higher than

that of Pt black. In addition, the size of the porous Pt dendrites can be controlled from 13 nm to 53 nm by adjusting the reaction temperature.⁴⁸ Recently, Jin and coworkers developed a universal approach to prepare Pt, Pd and Au nanodendrites.⁴⁹ An amino acid based surfactant, sodium *N*-(4-*n*-dodecyloxybenzoyl)-*L*-isoleucinate, was employed as the surfactant due to its pH-dependent self-assembly properties. The porous Pd, Pt and Au structures can be obtained by controlling the pH at 5.0 for the formation of vesicles of the surfactant.

In comparison to pure Pt metals, Pd–Pt bimetallic porous structures exhibited much better performance. Xia and co-workers prepared Pd–Pt dendrites through a seed-mediated growth method.⁵⁰ The 23.5 nm bimetallic nanodendrites consisted of a dense array of Pt branches on a core of truncated octahedral Pd (Fig. 2). Both homogeneous and heterogeneous nucleation of Pt occurred at very early stages of the synthesis. The truncated octahedral Pd seeds provided multiple nucleation sites for Pt atoms to attach on their surfaces.⁵¹ In addition, the introduction of Pd seeds helps avoid overlap and fusion between the Pt branches during the growth process. The porous particles showed a single crystalline structure, indicating a highly ordered orientation of Pd and Pt atoms. The exposed facets were concluded to be a mixture of {100}, {111} and {110}, together with some high-index facets. The mass activity of the porous structure is 2.5 times that of commercial Pt/C due to the high surface area and the exposure of particularly active facets. A similar Pd–Pt dendritic structure is obtained by reducing platinum(II) acetylacetonate (Pt(acac)₂) in a diphenylether/oleylamine mixture in the presence of preformed 5 nm Pd nanoparticles as seeds.⁵² The as-prepared Pt on Pd dendrites exhibited both excellent activity and stability towards the oxygen reduction reaction (ORR). To develop a one-pot synthesis of Pd–Pt porous structures instead of seed-mediated growth,

Yamauchi reduced Pt and Pd precursors simultaneously in the presence of Pluronic P123 as a surfactant.⁵⁴ Thanks to the different standard reduction potentials of Pd and Pt, the Pd cores formed first, followed by the deposition of Pt dendrites on the cores. By supporting the as-prepared Pt-on-Pd bimetallic dendrites on graphene nanosheets, the electrochemical performance of the catalysts can be further enhanced due to the improved dispersion and the interface between the metal and graphene. Based on this point, graphene/bimetallic nanodendrite hybrids were prepared by depositing Pd atoms on graphene nanosheets, followed by the selective deposition of Pt on Pd particles.⁵³ The size and different numbers of Pt branches can be precisely controlled by adjusting the amount of Pt precursor.

In addition to Pd–Pt bimetallic dendrites, several Pt-based porous structures with different compositions were fabricated. For instance, Wang *et al.* synthesized Pt-on-Au bimetallic dendrites through a one-step wet-chemical reduction route. The reduction kinetics for Pt is much slower than that of Au, which resulted in the formation of Au cores and Pt nanobranches.⁵⁸ Besides the doping of noble metals, 3d-transition metals were introduced by simultaneously reducing Pt and 3d-transition metal precursors. Li and co-workers prepared highly branched Pt–Ni nanocrystals by simultaneously reducing Pt(acac)₂ and Ni(acac)₂ at 250 °C.⁵⁹ Sun *et al.* demonstrated a facile one-pot synthetic strategy to produce PtFe and PtRuFe nanodendrites.⁶⁰ During the reaction, Fe atoms were formed at the initial stage; then galvanic replacement of Fe with Pt species in the solution led to the growth of PtFe alloyed dendrites. With the introduction of Ru precursors into the synthesis system, Ru could be co-reduced with Pt and alloyed into PtFe dendrites, forming ternary PtRuFe nanodendrites.

2.2 Pt-Based ultra-thin nanowires

Although nanoporous structures can maintain a high AUE for Pt catalysts, the exposed surface facets are complicated due to the uneven surface atom arrangement. Shape-controlled synthesis can obtain a nanocrystal with a smooth surface, which has specific facets exposed. Among various nanostructures, ultra-thin nanowires are considered a nanostructure with high AUE due to their extremely high length-diameter ratio.^{61–74} Lou and Wang fabricated ultrathin (3 nm) Pt nanowires by reducing chloroplatinic acid hexahydrate in a mixed solvent of KOH, *N,N*-dimethylmethanamide (DMF) and ethylene glycol.⁶³ The formation process of nanowires follows an oriented attachment mechanism instead of seed-mediated growth, with KOH playing an important role. In addition, the as-prepared nanowires tended to self-assemble into bundles with a diameter of 30 nm, due to their high surface energy. Ultra-thin Pt nanowires can also be prepared by symmetric growth from dumbbell seeds.⁶⁴ The length of the nanowires (with a uniform diameter of 2–3 nm) can reach up to several microns after the seed-mediated growth. In this case, the formation of dumbbell-like nuclei played a pivotal role in the formation of the Pt nanowires. In addition to the wet-chemical reduction method, ultra-thin Pt nanowires can be prepared by a modified phase-transfer method by using *n*-dodecyltrimethylammonium bromide as the phase-transfer agent.⁶⁵ The width of nanowires is controlled

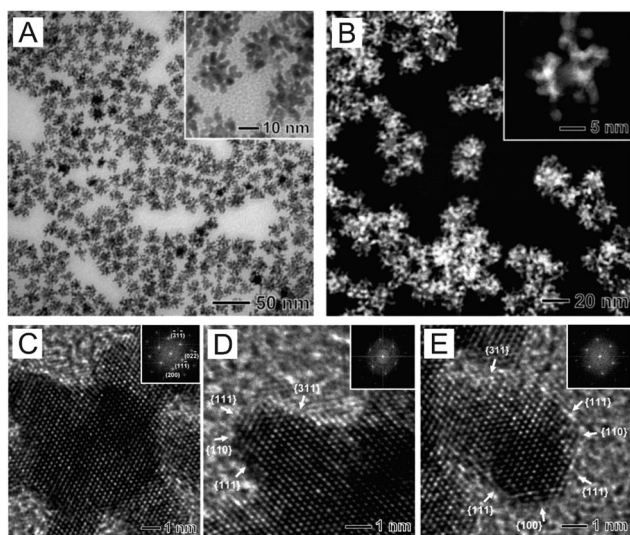


Fig. 2 (A and B) TEM and HAADF-STEM images of Pd–Pt nanodendrites synthesized through seed-mediated growth in an aqueous solution. (C–E) High-resolution transmission electron microscopy (HR-TEM) image recorded from the center and edge positions of one Pd–Pt nanodendrite. Adapted with permission from ref. 50. Copyright 2009 American Association for the Advancement of Science.

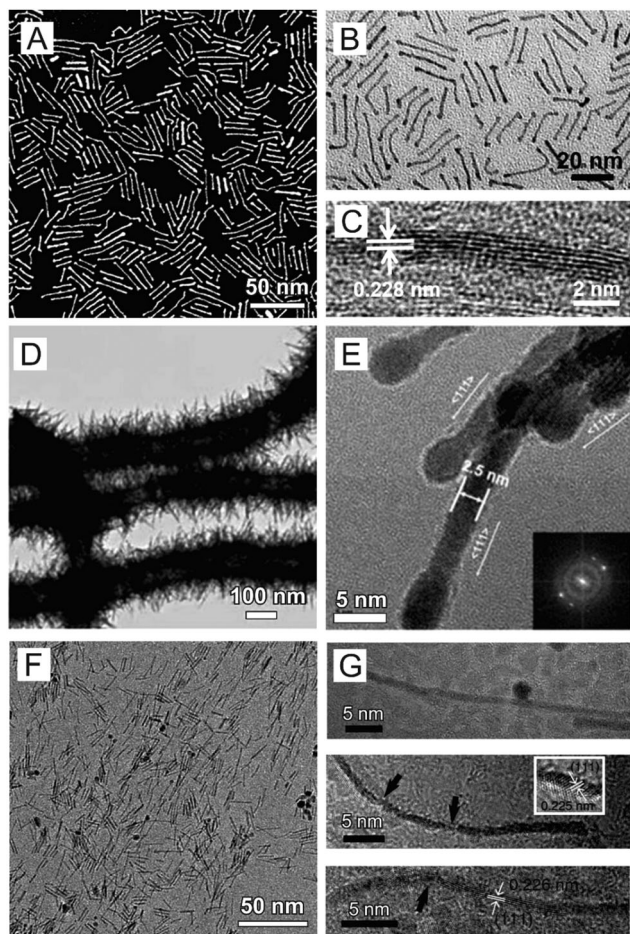


Fig. 3 (A–C) STEM image, TEM image and HR-TEM image of subnanometer Pt nanowires, respectively. Adapted with permission from ref. 66. Copyright 2017 American Association for the Advancement of Science. (D and E) TEM and HR-TEM images of ultrathin Pt nanowires grown on NCNT. Adapted with permission from ref. 68. Copyright 2009 Wiley-VCH. (F and G) TEM and HR-TEM images of Pt NWs on single-layer Ni(OH)₂. Adapted with permission from ref. 69. Copyright 2015 Nature Publishing Group.

to be 2.3 nm and the length is over 30 nm. In addition to pure Pt nanowires, Huang *et al.* prepared Pt, PtNi, PtCo and PtNiCo subnanometer alloy nanowires in an oleylamine system.⁶⁶ Four to five atom wide Pt nanowires can be obtained by using oleylamine as a reducing agent and cetyltrimethylammoniumchloride (CTAC) as the surfactant (Fig. 3A–C). To reduce Ni and Co precursors together with Pt, glucose is used as the reducing agent instead of oleylamine. The length of nanowires can be tuned from 9 nm to 35 nm by adjusting the amount of Mn(CO)₆. Thanks to the atomic level character and alloy effect, the as-prepared Pt-based alloy exhibited boosted ORR activity. In another study, by reducing Pt(acac)₂ with Fe(CO)₅ in the presence of oleylamine solution, PtFe ultra-thin nanowires can be prepared through a solution-phase reduction method.⁶⁷ In this case, the Pt/Fe composition of the nanowires can be tuned from 0.8 : 1 to 2.4 : 1; furthermore, the PtFe nanowires have a high electrochemical area of 52 m² g⁻¹ and a Pt utilization of 76%.

To avoid the aggregation of free-standing nanowires, the direct growth of Pt nanowires on active supports can effectively

improve the stability of Pt nanowires. Sun and co-workers synthesized ultra-thin Pt nanowires with a diameter of 2.5 nm and length of 100 nm on nitrogen-doped carbon nanotubes (N-CNTs) (Fig. 3D and E).⁶⁸ The Pt nanowires were grown on N-CNTs by a very simple aqueous solution method at room temperature. The defects associated with N incorporation in N-CNTs promoted Pt nucleation on the N-CNTs and the anisotropic growth of ultrathin nanowires. Tang *et al.* report a design strategy for the growth of Pt nanowires on two-dimensional single layered Ni(OH)₂ nanosheets (SL-Ni(OH)₂) (Fig. 3F and G).⁶⁹ In this reaction system, formamide acts as both the solvent for dispersing SL-Ni(OH)₂ nanosheets and the reducing agent for generation of Pt nanowires. The introduction of KOH increased the reducing ability of formamide, which aids the heterogeneous growth of 1D Pt nanowires. This Pt nanowire/SL-Ni(OH)₂ hybrid material exhibited 4–5 times higher HER activity in alkaline conditions compared to a commercial Pt/C catalyst.

2.3 Pt-Based core-shell structures with ultra-thin shells

Among various nanostructures, core-shell structures have exhibited unique properties due to their bimetallic character. Although many efforts have been made for the preparation of X-Pt (X = Cu, Au, Pd) core-shell structures, most of the as-prepared Pt shells are too thick (> 5 nm). It can be expected that when the thickness is reduced to less than 4 atomic layers, the AUE of catalysts can exceed 25%. To achieve an ultra-thin Pt shell, Adzic and co-workers developed a method for depositing Pt monolayers involving the galvanic displacement by Pt of an underpotentially deposited (UPD) Cu monolayer on a Pd substrate.⁷⁵ A full monolayer of Cu can be deposited on Pd through electrodeposition, with Pt atoms being irreversibly deposited onto the Pd substrates through a galvanic replacement reaction. During the Pt deposition process, the UPD Cu layer lowers the rate of Pt deposition and enhances surface diffusion of Pt adatoms, resulting in a smooth Pt monolayer.⁷⁶ As the Pt shell is very thin, the properties of the Pt monolayer may be greatly influenced by the core material. By changing the Pd core to Pd₉Au₁, the stability of Pt monolayer catalysts was significantly enhanced. The Pt/Pd₉Au₁ catalysts showed minimal degradation in mass activity (only 8%) over 100 000 cycles durability test; while the Pt/Pd electrocatalyst declined to 37% after 100 000 cycles.⁷⁷ In addition, Liao and co-workers prepared Pd₁Ru₁Ni₂ alloy nanoparticles as the core by a chemical reduction method for the deposition of a Pt monolayer. They found that the addition of Ni to the core played an important role in enhancing the oxygen reduction activity and stability.⁷⁸

In addition to the galvanic replacement reaction method, Liao and Adzic reported a pulsed electrodeposition method for direct growth of ultra-thin Pt layers on TiNiN substrates.⁷⁹ The Pt catalyst was deposited on a TiNiN support, which avoids carbon-support corrosion. Besides the pulsed electrodeposition method, Toyoda *et al.* fabricated an epitaxial Pt thin film with a thickness of 1.5 nm on a TaB₂(0001) single-crystal substrate by vacuum deposition at room temperature.⁸⁰ With the electronic effect of Ta on Pt, the d-band center for the PtTa alloy is lower than pure Pt, thus the as-prepared Pt/TaB₂ exhibited enhanced

ORR specific activity (normalized by the ECSA). Moreover, with the formation of an ultra-thin Pt shell, the mass activity is six times higher than that of Pt/C.

The wet-chemical reduction method is also an effective route for the preparation of uniform ultra-thin Pt shells. However, during the direct growth of Pt shells through wet-chemical reduction, the Pt atoms often take an island growth mode because of strong bonding between Pt atoms. To avoid the self-nucleation of Pt atoms, Xia and co-workers introduced a solution-phase method for the conformal deposition of

ultrathin shells of Pt on Pd nanocrystals with control on the atomic scale.^{81,82} A high temperature (200 °C) and slow injection rate of Pt precursors are key for the formation of Pd@Pt core-shell structures with smooth Pt shells. The atomic layers of Pt can be precisely controlled from 1 to 8 layers by adjusting the amount of Pt precursor. As shown in Fig. 4A–C, the Pt atoms are evenly deposited on Pd nanocubes, maintaining the initial core surface structure. The growth mechanism contains two steps: the deposition of Pt atoms at the corner of Pd cubic seeds and the diffusion of Pt atoms from corners to surfaces.

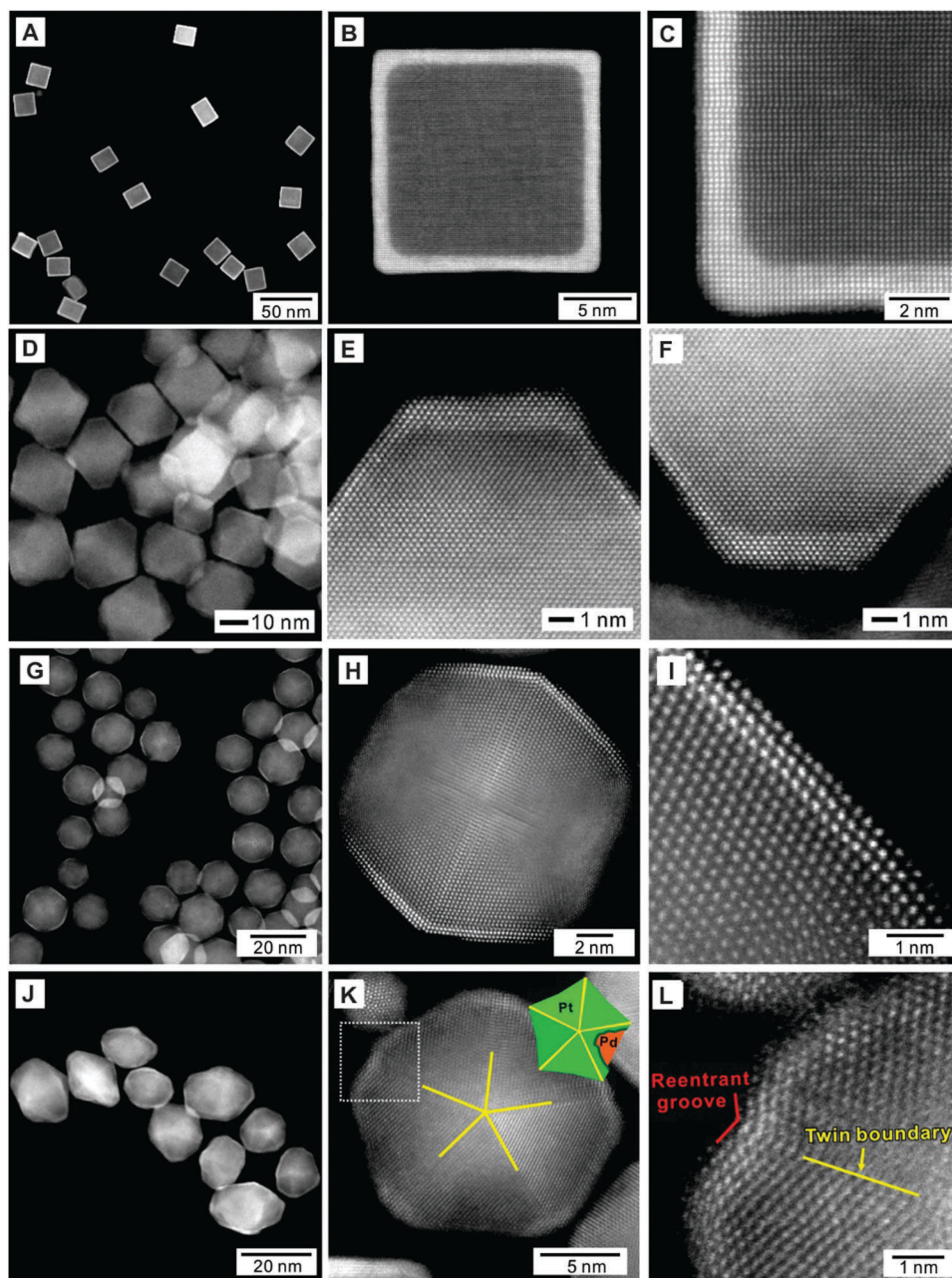


Fig. 4 Low-magnification HAADF-STEM images, HAADF-STEM images of individual particles and atomic-resolution HAADF-STEM images of four Pd@Pt core-shell structures with different morphologies: (A–C) nanocubes; (D–F) octahedrons; (G–I) icosahedrons; (J–L) decahedrons. Adapted with permission from ref. 81 (Copyright 2014 American Chemical Society), 86 (Copyright 2015 American Chemical Society), 89 (Copyright 2015 Nature Publishing Group) and 91 (Copyright 2015 American Chemical Society).

The diffusion rate is greatly dependent on the reaction temperature and when the reaction was carried out at 180 °C, the products exhibited a concave structure. Thanks to the ultra-thin shell, the large Pd@Pt core-shell structures (~20 nm) exhibited higher mass activity compared with commercial Pt/C. In addition to catalyzing the ORR, the cubic Pd@Pt catalysts were also applied to the HER and photocatalytic water splitting. The ultra-thin Pt shell provided an opportunity to investigate the surface polarization mechanism for enhanced HER performance of Pt catalysts.⁸³ By depositing the cubic Pd@Pt catalysts on TiO₂, the well-designed nanocrystals acted as good co-catalysts for photocatalytic water splitting.⁸⁴

As {111} facets exhibit higher ORR activity than {100} facets, the growth system was extended to the preparation of octahedral Pd@Pt catalysts.⁸⁵ Because Pd(111) has a much lower surface free energy than Pd(100), the injection rate must be slower than that for preparation of cubic structures to avoid the formation of Pt clusters. The Pd@Pt octahedra can be obtained in aqueous systems at a much lower temperature by using a weak reducing agent.⁸⁶ As shown in Fig. 4D–F, the Pt atoms prefer to deposit on {100} sites due to the relatively higher surface energy of {100} facets. When using Pd nanoplates as the seeds, two different types of Pd@Pt nanoplates can be fabricated by using polyol- and water-based protocols. In contrast to cubic and octahedral seeds, the surface energy of the side faces is much higher than the top surface due to the presence of twin boundaries. As a result, evenly covered Pd@Pt nanoplates can be obtained in a polyol-system due to the high atom diffusion rate; while the Pt atoms only selectively deposited on the side faces in water-based protocols.⁸⁷

The catalytic activity of Pd@Pt core-shell structures with high AUE can be further increased through Pd seeds with twin defects. With the introduction of surface strain, the binding properties of adsorbates can be modified. For instance, Yang and coworkers reported that the specific activity (normalized by the ECSA) of Pt₃Ni icosahedra, whose surface was under a tensile strain, was 1.5 times that of Pt₃Ni octahedra with a similar size.⁸⁸ Therefore, the combination of high AUE, {111} facets and twin defects can enhance the ORR activity further than any singular effect. With the deposition of Pt atoms on Pd icosahedrons, the Pt overlayers are forced to evolve into a compressed, corrugated structure due to the lateral confinement imposed by the boundaries of twin defects (Fig. 4G–I). Density functional theory (DFT) calculation results showed that the introduction of a compressive strain weakens the binding energy of OH, allowing the Pd@Pt_{nL} icosahedra to exhibit substantial improvement in both activity and durability towards the ORR.⁸⁹ Similar to icosahedra, Pd decahedra also contain the boundaries for twin defects, which may have strong ORR performance.^{90,91} Yang *et al.* reported a facile approach that allows one-pot epitaxial growth of a uniform Pt shell on Au decahedral cores with a starlike geometry.⁹⁰ The introduction of an amine decreased the surface energy of Pt, promoting epitaxial growth on the Au cores. In addition, Xia and co-workers prepared Pd@Pt decahedra with twin boundaries as shown in Fig. 4J–L.⁹¹ The as-prepared Au–Pt and Pd–Pt decahedra catalysts both exhibited better ORR performance

than Pt/C, due to the strong electron interaction arising from a lattice-matched interface.

2.4 Pt-Based hollow structures

2.4.1 Pt-Based nanocages with subnanometer walls.

Generally, nanocage structures can be fabricated by a galvanic replacement reaction, with Ag nanocubes being widely used as the seeds for fabrication of Au, Pd and Pt nanocages.^{92,93} The sizes and shapes of the Pd and Pt nanocages are determined primarily by the Ag nanocube sizes and reaction temperatures.⁹⁴ Pd seeds can also be used as the seeds for the preparation of Pt-based nanocages. For example, Han and co-workers prepared cubic and octahedral Pt nanocages with 8 nm thick walls.⁹⁵ However, the thickness of nanocages prepared from galvanic replacement or one-pot synthesis is too large, with a low AUE. To obtain nanocages with ultra-thin walls, an effective route is to fabricate core-shell structures, followed by the selective etching of interior cores. Thanks to the successful preparation of Pd@Pt core-shell nanostructures with ultra-thin shells, cubic and octahedral Pt nanocages with subnanometer-thick walls can be obtained by selectively etching Pd cores with FeCl₃ and HCl (Fig. 5A–D).⁹⁶ These nanocages are approximately 6–7 atomic layers thick. The formation of a channel to dissolve the Pd atoms was the key for the generation of nanocages. DFT results showed an energy barrier of 0.99 eV for the diffusion of Pt adatoms across a Pd(100) surface. In contrast, a Pt adatom can substitute into the Pd surface, with a barrier of just 0.74 eV, which means that some Pd atoms will be incorporated into the Pt shell (Fig. 5E). Upon contact with the etchant, the Pd atoms in the outermost layer are oxidized to generate surface vacancies. The underlying Pd atoms then diffuse to these vacancies and are continuously etched away, leaving behind atom-wide channels (Fig. 5F). The morphology of nanocages is highly dependent on the Pd@Pt core-shell structure. For example, plate-like Pt nanocages and Pt nanorings are obtained from the Pd@Pt nanoplates prepared in polyol and water-based systems, respectively.⁸⁷

Pt-based icosahedral nanocages whose surfaces are enclosed by both {111} facets and twin boundaries were prepared using Pd@Pt icosahedra as seeds (Fig. 6).^{97,98} During the selective etching of Pd cores, the Pt atoms on the shell reconstruct and the lateral confinement imposed by the twin boundaries no longer exists in the nanocage structure (Fig. 6E). Thanks to the synergistic effect of {111} facets, twin defects, and ultrathin walls, the icosahedral nanocages exhibited a mass activity of 1.28 A mg⁻¹, which is 6 times that of Pt/C catalysts. Unlike the coating of a Pd icosahedral seed, the Pt atoms prefer to stay at the vertices and edges/ridges of a decahedral seed even when the deposition is conducted at 200 °C, naturally generating a core-shell structure covered by concave facets.⁹¹ After the etching process of the concave decahedra, some of the {111} facets were etched away, whereas the majority of Pt atoms on the edges/ridges and vertices of the decahedra were retained.

2.4.2 Pt-Based nano-frame structures. Similarly, Pt-based nanoframes can also be obtained through a seed-growth and selective etching method, using Au nanoparticles as seeds.^{99,100} However, the as-prepared Pt nanoframes (nanorings, nanowires)

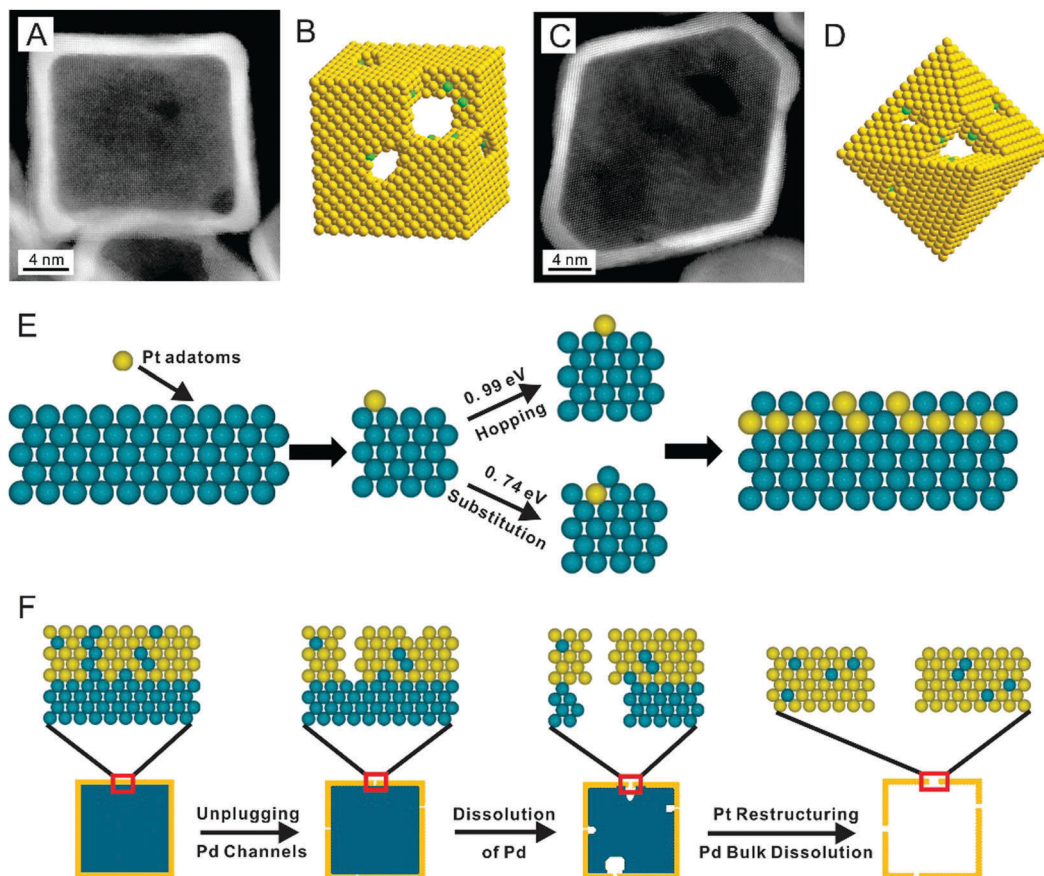


Fig. 5 (A and B) STEM image and corresponding atomic model of Pt cubic nanocages. (C and D) STEM image and corresponding atomic model of Pt octahedral nanocages. (E) Schematic illustrations showing interdiffusion of deposited Pt atoms and Pd cores. (F) Schematic of the major steps involved in the continuous dissolution of Pd atoms from a Pd@Pt cube to generate a Pt cubic nanocage. Adapted with permission from ref. 96. Copyright 2015 American Association for the Advancement of Science.

have thick edges. Contrasting with the fabrication of ultra-thin nanocages, most of the nanoframe structures with high AUE are obtained through one-pot synthesis.^{101–116} In addition, with the synergistic effect of composition and high AUE, the as-prepared Pt-based nanoframe structures exhibit excellent electrochemical performance in both anode and cathode related reactions.

For example, Yang and Stamenkovic prepared Pt–Ni nanoframes by corroding the PtNi₃ rhombic dodecahedrons in hexane, followed by a thermal treatment in an inert gas (Ar) atmosphere at 370 °C.¹⁰⁴ The as-prepared hollow Pt₃Ni nanoframes with Pt-rich skin contain 24 2 nm-thick edges that retain the high crystallinity of the parent structure (Fig. 7). Li *et al.* reported an efficient method for synthesizing Pt–Ni nanoframes by transforming truncated octahedral Pt–Ni alloy particles through a priority-related chemical etching process.¹⁰⁵ The corresponding DFT calculation results showed that the diffusion rate of Ni atoms at (100) facets is faster than Pt atoms, providing a channel for chemical etching of the cores. In addition, the etching mechanism followed the Kirkendall effect stemming from distinct diffusion coefficients of Ni and Pt. Jung and Lee prepared a phase-segregated octahedral PtNi nanoparticle at 170 °C under 1 atm of CO.¹⁰⁶ With the introduction of sodium oleate into the reaction system, the Ni shell growth was interrupted

due to the coordination effect between Ni and sodium oleate, resulting in a nanoframe structure.

In addition to PtNi bimetallic nanoframes, studies about the shape-controlled preparation of PtCu structures attract more and more attention due to their good electrochemical performance in methanol oxidation and formic acid oxidation. Among them, various types of PtCu nanoframes were prepared in recent years. Lou and co-workers prepared cubic PtCu₃ nanoframes by reducing H₂PtCl₆·6H₂O and Cu(acac)₂ in the presence of cetyltrimethylammonium bromide (CTAB) and oleylamine at 170 °C for 24 h (Fig. 8A).¹⁰⁷ In this case, CTAB was found to affect the reduction rate of Pt and Cu species and Cu atoms were first to be reduced. The following galvanic replacement of Cu nanocrystals with Pt species in the solution finally leads to the formation of PtCu₃ hollow nanoframes. Octahedral Pt–Cu nanoframes were prepared in a polyvinylpyrrolidone (PVP), glycine, NaI and ethanolamine system, with the latter two playing a significant role as surface controllers for the octahedral structure (Fig. 8B).¹⁰⁸ The introduction of glycine above a certain amount can influence the reduction rates of Pt and Cu species, promoting the formation of nanoframe structures. In addition to the cubic and octahedral nanoframes, excavated rhombic dodecahedral (ERD) PtCu₃ alloy nanoframes were

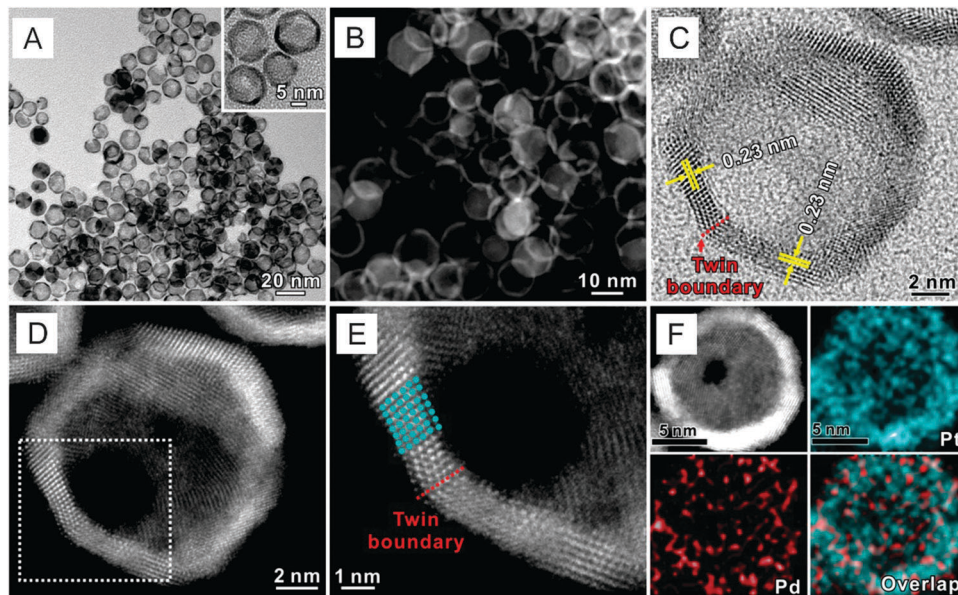


Fig. 6 (A) TEM and (B) low-magnification HAADF-STEM images of the Pt icosahedral nanocages. (C) Bright-field and (D, E) atomic-resolution HAADF-STEM images taken from a single nanocrystal. (F) HAADF-STEM image of an icosahedral nanocage and the corresponding energy-dispersive X-ray (EDX) mapping of Pd and Pt. Adapted with permission from ref. 97. Copyright 2016 American Chemical Society.

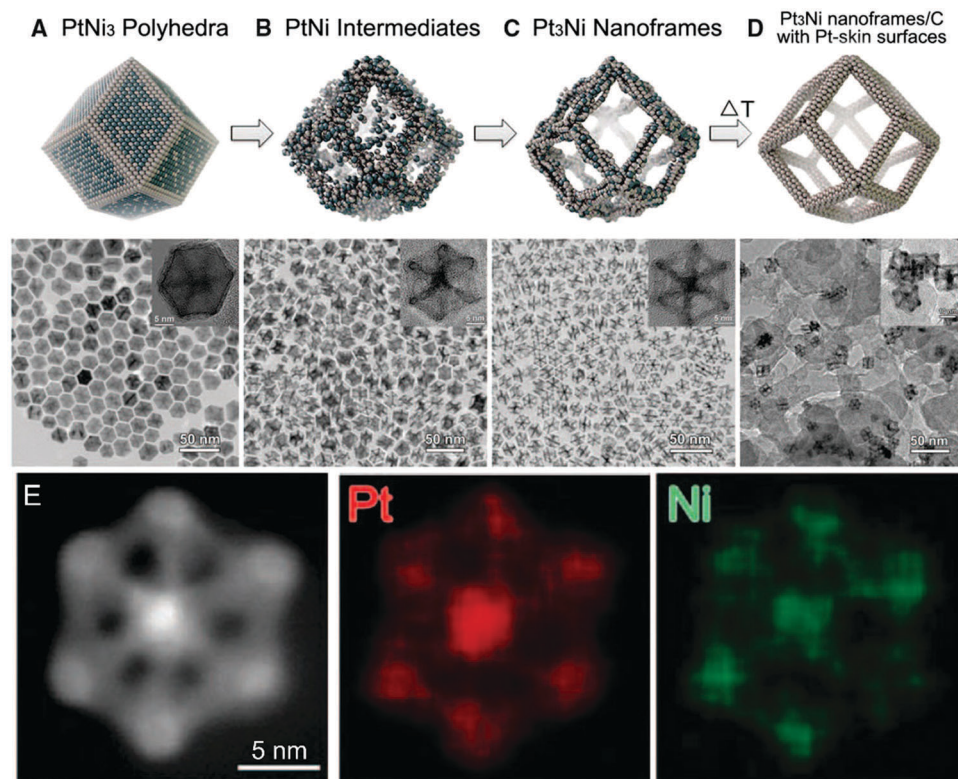


Fig. 7 (A–D) Schematic illustrations and corresponding TEM images of the Pt–Ni bimetallic nanocrystals obtained at four representative stages during the evolution process. (E) EDX elemental mapping results for Pt₃Ni nanoframes. Adapted with permission from ref. 104. Copyright 2014 American Association for the Advancement of Science.

prepared in DMF solution in the presence of *n*-butylamine and CTAC (Fig. 8C–F).¹⁰⁹ The controlled experiments showed that *n*-butylamine can selectively adsorb on {110} facets, resulting in

the rhombic dodecahedron geometry. Differing from the galvanic replacement of Cu with Pt atoms, the excavated rhombic dodecahedral PtCu₃ forms due to block growth along

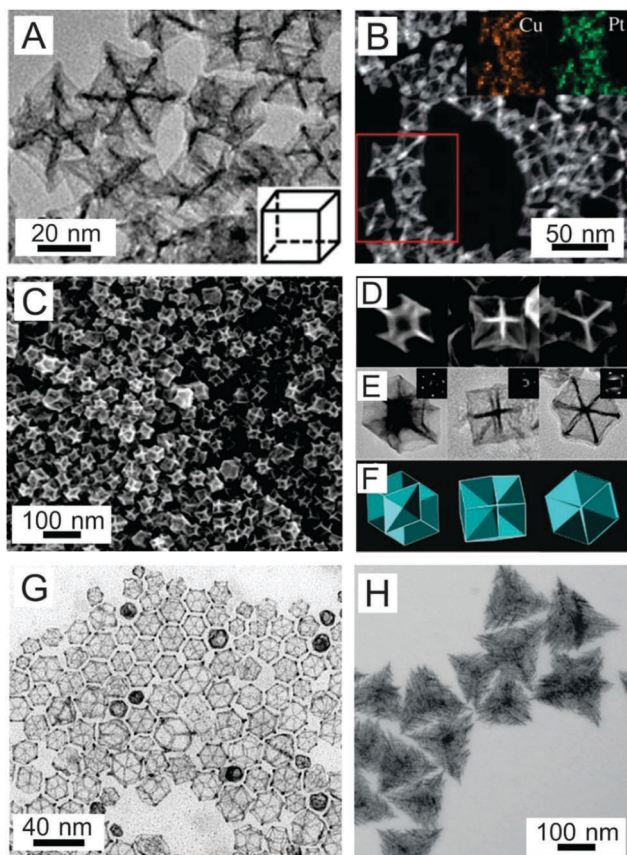


Fig. 8 (A) HR-TEM image of PtCu₃ cubic nanoframes. Adapted with permission from ref. 107. Copyright 2012 American Chemical Society. (B) HAADF-STEM image of octahedral Pt-Cu nanoframes. Adapted with permission from ref. 108. Copyright 2013 Royal Society of Chemistry. (C–F) Characterization of ERD PtCu₃ alloy nanocatalysts. Adapted with permission from ref. 109. Copyright 2014 American Chemical Society. (G) TEM image of rhombic dodecahedral PtCu nanoframes. Adapted with permission from ref. 110. Copyright 2015 Wiley-VCH. (H) TEM image of Pt-Cu HTBNs. Adapted with permission from ref. 111. Copyright 2015 Wiley-VCH.

{110} edges of the octahedral seeds. Meanwhile, the {110} facets are stabilized, causing the formation of {110} facets in the octahedral corner area. Alternatively, Guo and Huang report a facile method for the preparation of highly open rhombic dodecahedral PtCu alloy nanoframes (Fig. 8G).¹¹⁰ The as-prepared PtCu bimetallic catalysts exhibit enhanced performance in methanol oxidation. Furthermore, Zeng *et al.* prepared novel ordered Pt-Cu alloy hierarchical trigonal bipyramidal nanoframes (HTBNFs) in an ethylene glycol system (Fig. 8H).¹¹¹ The Cu UPD atoms on the surface forced the atoms to selectively deposit on the corner of plate-like seeds forming the HTBNF structure. In addition, the particle size can be controlled from 110 nm to 250 nm by tuning the introduced amount of KI.

3. Pt clusters and single atom catalysts

3.1 Pt clusters and their size effects on performance

For the evaluation of catalytic performance, the specific activity and mass activity are two important factors. The specific

activity is usually normalized by the ECSA, and is greatly dependent on the surface active sites of the catalyst. In contrast, the most important route for improving the mass activity is to obtain high AUE catalysts. The direct way to improve the AUE is to decrease the particle size of Pt catalysts. Based on this point, several studies have investigated the relationship between Pt catalyst particle size and the catalytic performance.^{117–122}

Shao and co-workers prepared a series of Pt catalysts with different particle sizes on a carbon support by replacing the Cu under-potential-deposition (UPD) layer with Pt atoms.¹¹⁷ The average particle sizes of the catalysts can be controlled to be 1.3, 1.84, 2.46, and 4.65 nm as shown in Fig. 9. They simulated that the truncated octahedral particles between 0.8 and 3 nm had 38, 79, 116, 201, 314, 586, and 807 total Pt atoms, respectively. The electrochemically active surface area increases gradually with the decrease in particle size. However, the mass activity and specific activity of the catalysts did not increase with the improvement in AUE. The specific activity of the catalysts with an average particle size larger than 2.2 nm was 4 times larger than that of 1.3 nm catalysts. The obvious increase in specific activity can be attributed to the increase in the number of {111} active sites. With the size of Pt catalysts further increasing, the activity slightly increased from 0.11 mA cm⁻² to 0.13 mA cm⁻² due to the increase of {111} facets. Differing from the trend of specific activity (normalized by the ECSA), the 2.2 nm catalysts exhibited the best mass activity and the performance decreased with larger particle sizes. It is evident that the best ORR mass activity results from the combination of a high ratio of {111} surface sites and a high AUE. Arenz and co-workers employed a Pt-black catalyst, a polycrystalline Pt sample and four high

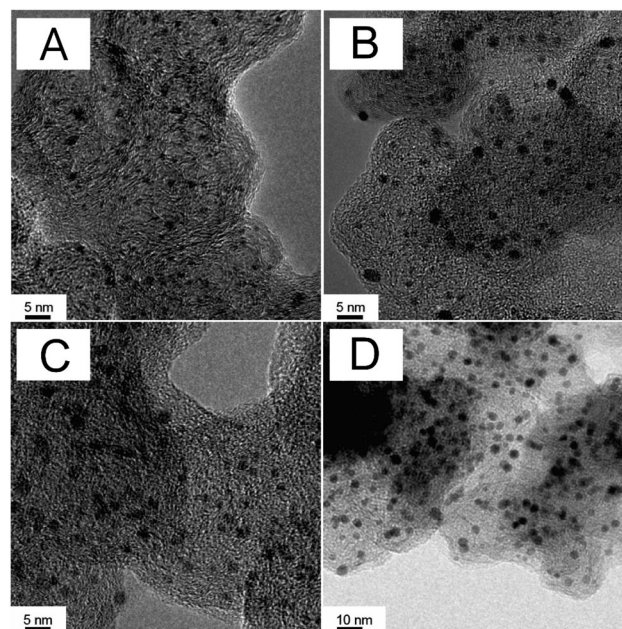


Fig. 9 TEM images of Pt particles with various sizes, which were supported on carbon black. The average particle sizes for (A), (B), (C), and (D) are 1.3, 1.84, 2.46, and 4.65 nm, respectively. Adapted with permission from ref. 117. Copyright 2011 American Chemical Society.

surface area carbon supported catalysts with sizes of 1 nm, 2 nm, 2–3 nm and 4–5 nm to examine the influence of the size of Pt nanoparticles on the ORR performance.¹¹⁸ They found that the activity trend for the ORR performance is independent of the electrolyte. The specific activity (normalized by the ECSA) rapidly decreases going from polycrystalline Pt to unsupported Pt black particles and HSA carbon supported Pt NPs. The mass activity exhibited the opposite trend compared to the specific activity, indicating that the AUE performs a significant role for improving the mass activity of the catalysts. Shao-Horn *et al.* examine the ORR activity of carbon supported Pt catalysts with particle sizes ranging from 1.6 nm to 4.7 nm in HClO₄ and H₂SO₄.¹¹⁹ To generate particles with larger diameters, the Pt/C catalyst containing 46% Pt nanoparticles was further treated in Ar at 900 °C for one minute or two hours. The Pt/C catalysts exhibited a five-fold reduction in the specific ORR activity in H₂SO₄ relative to HClO₄, due to the strong adsorption of sulfate. In addition, the specific activities of the catalysts are similar at 0.9 V vs. RHE (reversible hydrogen electrode). They mentioned that the specific ORR activity on majority terrace sites is much greater than those of minority under-coordinated sites, which is responsible for the size-independent activity. The mass activity increased with smaller particle sizes, due to the greatly increased AUE.

3.2 Pt single atom catalysts

As the AUE scales with particle size, a maximum efficiency of 100% can be reached when the Pt catalysts are reduced to single atoms. Recently, different single atom catalysts have been developed through photochemical reaction, wetness impregnation, and atomic layer deposition methods *etc.*^{123–133} With the formation of single atom catalysts, the Pt single atom catalysts exhibited distinct catalytic performance when compared to Pt nanoparticles.

3.2.1 Wetness impregnation method. Wetness impregnation is a commonly used preparation method for the synthesis of heterogeneous catalysts. In a typical preparation process, the active metal precursor is dissolved in an aqueous solution and mixed with a catalyst support. The mixture can be dried and calcined to drive off the volatile components within the solution, depositing the metal on the catalyst surface (Fig. 10A). When the loading amount of metal is reduced to a very low level, single atom catalysts can be obtained on the support.¹³⁴ In addition, the uniformity of the single atom catalyst dispersion is also highly dependent on the precursor–support interactions that occur through chemical or physical forces. Therefore, the selectivity of the support is very important.

Lee and co-workers employed TiN nanoparticles as the support and obtained Pt single atoms through an incipient wetness impregnation method.¹³⁵ The Pt single atom catalysts

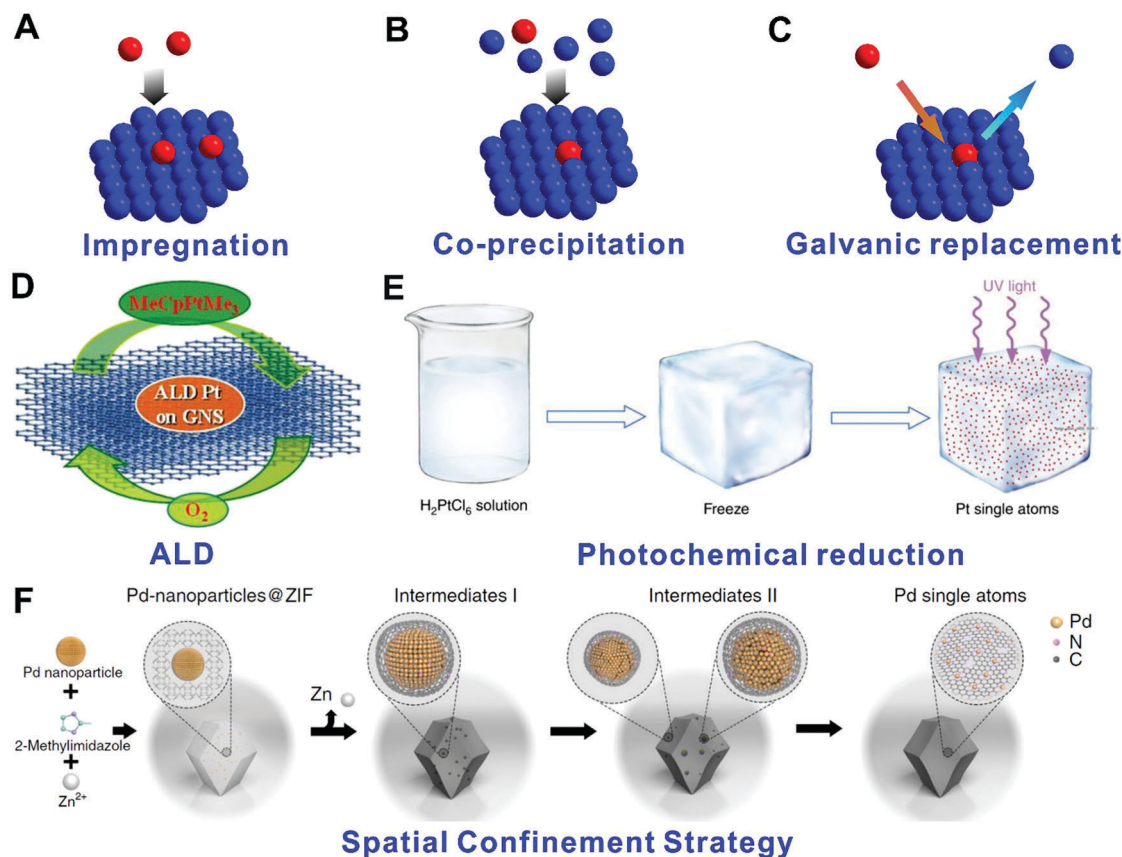


Fig. 10 Summarized synthetic methods for the preparation of Pt single atoms. Adapted with permission from ref. 127 (Copyright 2013 Nature Publishing Group), 144 (Copyright 2017 Nature Publishing Group) and 147 (Copyright 2018 Nature Publishing Group).

can be observed at a very low loading amount of 0.35 wt%; while Pt nanoparticles formed at higher mass loadings (2 and 5 wt%). DFT calculations indicated that Pt single atoms can be stabilized on an N-vacancy site on the TiN support. In addition to the TiN support, g-C₃N₄ was an effective support for anchoring Pt single atoms through impregnation. The N/C-coordinating framework of g-C₃N₄ can facilitate the binding of Pt atoms into the matrix, providing a potential scaffold for trapping the active Pt single atoms. Wu *et al.* prepared 0.16 wt% loading Pt single atoms on g-C₃N₄ by mixing g-C₃N₄ with H₂PtCl₆ followed by annealing at a low temperature.¹³⁶ The high-angle annular dark-field scanning transmission electron microscopy (HAADF-STEM) image and extended X-ray absorption fine structure (EXAFS) spectroscopy clearly confirmed the dispersion of Pt single atoms on the g-C₃N₄ network (Fig. 11). The as-prepared Pt₁/C₃N₄ catalysts exhibited enhanced photocatalytic H₂ generation performance compared to Pt nanoparticles. Sun *et al.* successfully prepared Pt single atoms on N-doped carbon black with a Pt loading of 0.4%. In this preparation, carbon black, urea and H₂PtCl₆ were used as a support, and N and Pt precursors, respectively. The mixed powder was then pyrolyzed at 950 °C for 1 hour, resulting in Pt single atoms on the support.¹³⁷ The Pt single atoms on N-doped carbon black were confirmed by scanning transmission electron microscopy (STEM) and synchrotron analysis. When no N is doped into the carbon support, Pt nanoparticles are also formed together with individual Pt atoms. These results indicated that pyridinic-N sites are a strong anchoring point for the deposition of Pt atoms. In addition,

DFT calculations showed that the single-pyridinic-nitrogen-atom-anchored Pt single atom centres are the main active sites, which greatly improved the electrochemical performance.

Although the wetness impregnation method is a simple and economical method for the preparation of single atom catalysts, the Pt loading amount is very low. To solve this problem, Li and co-workers prepared Ni(OH)_x with abundant vacancy defects to stabilize Pt single atoms. The Pt loading amount can reach 2.3 wt%.¹³⁸ Choi and co-workers employed S-doped zeolite-templated carbon as a support to fabricate Pt single atom catalysts with higher loading (5 wt%).¹²⁶ The Pt/high S-content zeolite-templated carbon catalysts (Pt/HSC) were prepared by a conventional wet-impregnation method, followed by H₂ reduction. EXAFS spectroscopy shows no appreciable Pt–Pt coordination, indicating the formation of a uniformly dispersed Pt single atom catalyst. Interestingly, the as-prepared Pt/HSC exhibited selectivity for a two-electron ORR pathway producing H₂O₂, instead of a four-electron pathway like most Pt catalysts.

3.2.2 Co-precipitation method. The co-precipitation method is also an effective route for the fabrication of single atom catalysts (Fig. 10B). Zhang *et al.* prepared Pt single atoms on FeO_x by co-precipitation of an aqueous solution of chloroplatinic acid and ferric nitrate (Fig. 12A and B).¹²⁵ In this case, Pt single atoms can be achieved with a loading of 0.17 wt%. When the Pt loading is increased to 2.50 wt%, Pt clusters consisting of 10 Pt atoms formed (Fig. 12C and D). The FeO_x support played a significant role for the performance enhancement of the Pt single atom catalysts. With the formation of a Pt–FeO_x interface, the electrons transfer from Pt

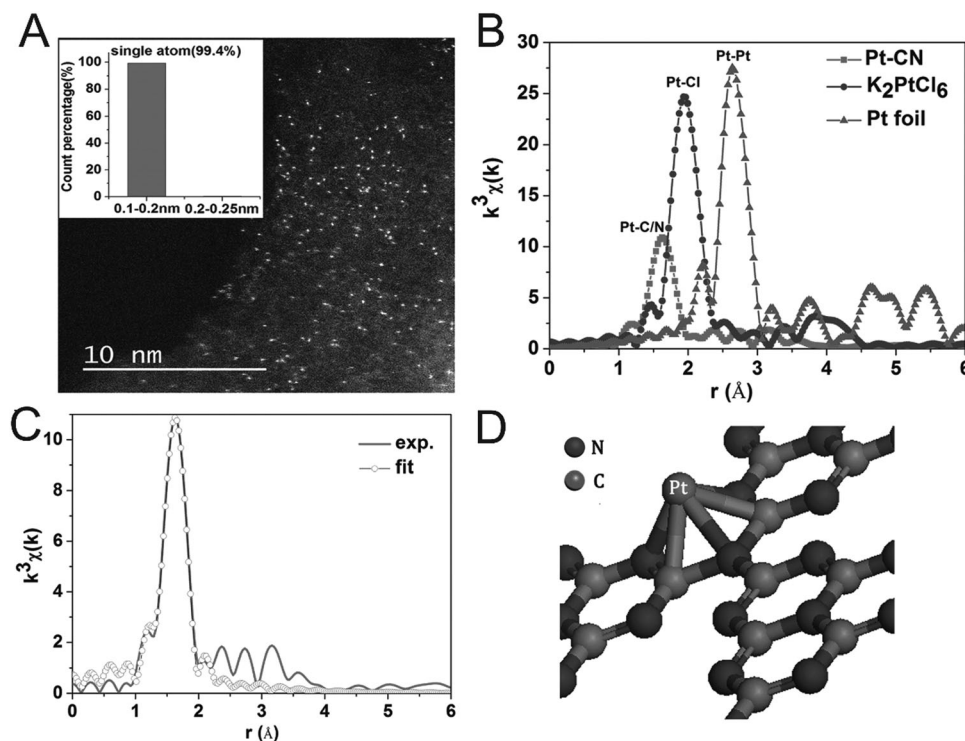


Fig. 11 (A) HAADF-STEM image of Pt single atoms on g-C₃N₄. (B) Fourier transforms of the Pt L3-edge EXAFS oscillations of Pt/g-C₃N₄, K₂PtCl₆, and Pt foil. (C) Comparison of EXAFS curves between the experimental data and the fit of the Pt single atoms on g-C₃N₄. (D) Schematic models of Pt-C₃N₄. Adapted with permission from ref. 136. Copyright 2016 Wiley-VCH.

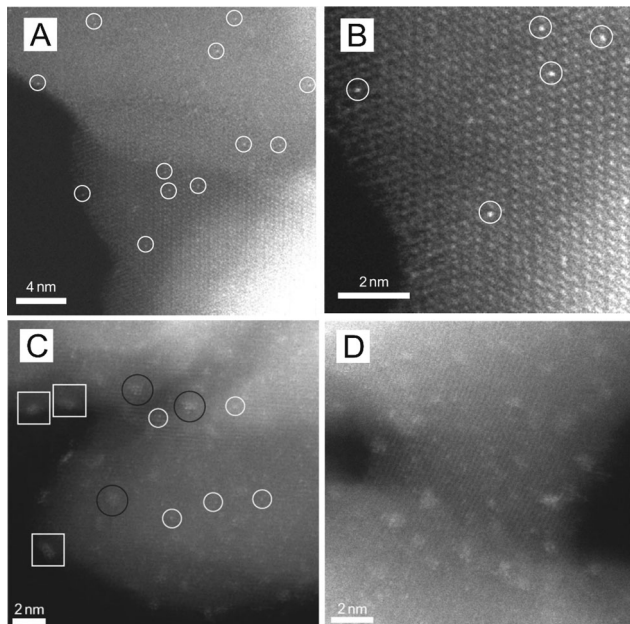


Fig. 12 (A and B) HAADF-STEM images of Pt single atoms on the FeO_x support. (C and D) HAADF-STEM images of Pt single atoms, together with two-dimensional Pt rafts consisting of fewer than 10 Pt atoms (black circles) and three dimensional Pt clusters of size about 1 nm. Adapted with permission from ref. 125. Copyright 2011 Nature Publishing Group.

atoms to the FeO_x surface, inducing positively charged Pt atoms and strong binding of Pt single atoms. As a result, the as-prepared Pt_1/FeO_x catalysts exhibited greatly enhanced CO oxidation performance.

Besides, Zhang's group has also achieved Ir single atom catalysts using the co-precipitation method.^{139,140} The as-prepared single atom catalysts are widely applied in CO oxidation, hydrogenation, water gas shift and oxidation of carbon monoxide reactions. However, the co-precipitation method is difficult for synthesis of single atoms on supports other than metal oxides. This is limiting, as metal oxide supports are not suitable for electrochemical testing due to their low conductivity and weak stability under acidic conditions.

3.2.3 Atomic layer deposition method. In addition to traditional wet-chemical preparation methods, atomic layer deposition (ALD) is a powerful approach for preparation of single atom catalysts. Moreover, it is also helpful for studying the relationship between the catalysts' structure and their catalytic performance, as it is able to precisely control the deposition of single atoms and nanoclusters.

In 2013, Sun and co-workers first fabricated single atoms and sub-nanometer clusters of Pt on the surfaces of a graphene nanosheet support through ALD.¹²⁷ During the ALD process, the Pt precursor (methylcyclopentadienyl)-trimethylplatinum (MeCpPtMe_3) first reacted with the adsorbed oxygen on the surface of graphene to form CO_2 , H_2O and hydrocarbon fragments. Then the subsequent oxygen will convert the precursor ligands to Pt–O species to form a new adsorbed oxygen layer on the Pt surface (Fig. 10D). During the whole ALD process, the Pt loading amount and particle size can be precisely controlled by adjusting the

number of ALD cycles. After 50 ALD cycles, the Pt single atoms are dominantly distributed on the surface of graphene nanosheets. With more ALD cycling up to 100 and 150 cycles, the particle size increased from single atoms to 1–2 nm and 4 nm, respectively. Due to more low-coordination and unsaturated 5d orbitals of the Pt single atoms, the catalysts showed much higher activity for methanol oxidation and superior CO tolerance compared to the commercial Pt/C catalyst. Very recently, Sun and co-workers deposited Pt atoms on nitrogen-doped graphene nanosheets (NGNs) instead of graphene, and the Pt single atom catalysts exhibited extremely high performance for the hydrogen evolution reaction (HER).¹²⁸ As shown in Fig. 13A, numerous individual Pt atoms, as well as very small Pt clusters, are uniformly dispersed on the NGNs for the ALD50Pt/NGN catalysts. After 100 ALD cycles, some Pt clusters grew to particles as shown in Fig. 13B. DFT calculation results showed that the Pt atom prefers to directly bond to the N-dopant (Fig. 13C). In addition, the Pt single atoms are mixed with the N-2p orbitals around the Fermi level, inducing a positive charge on the Pt atoms. As a result, the Pt single atoms on the N-doped graphene contain more unoccupied 5d orbitals. In addition, the X-ray absorption near edge structure data showed that the ALD Pt atoms have a high density of unoccupied 5d states, which agrees well with the partial density of states calculation. Thanks to the high AUE and the unique electronic structure originating from the adsorption of the Pt single atoms on the N-doped graphene, the mass activity of the ALD50Pt/NGN catalyst was much higher than the Pt/C catalyst towards the HER.

In addition to Pt single atom catalysts, Lu and co-workers precisely synthesized Pt dimers on graphene through ALD.¹⁴¹ The Pt dimers are obtained by depositing Pt single atoms on

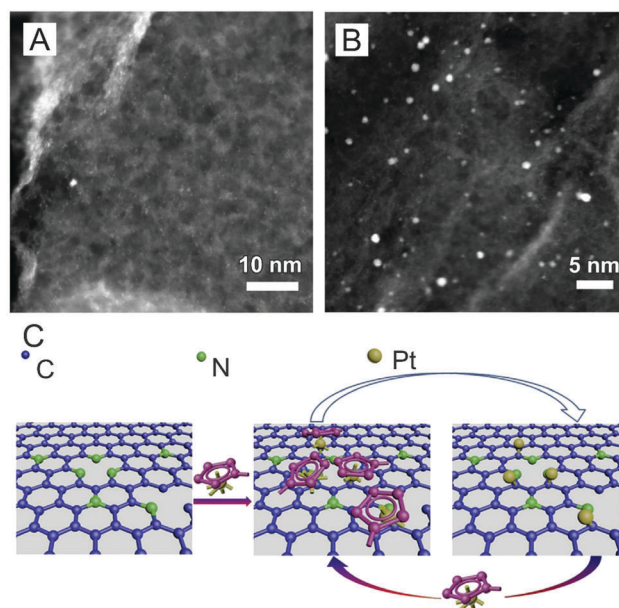


Fig. 13 (A and B) Annular dark field STEM images of ALD Pt/nitrogen-doped graphene nanosheet (NGN) samples with (A) 50 and (B) 100 ALD cycles. (C) Schematic illustration of the Pt ALD mechanism on NGNs. Adapted with permission from ref. 128. Copyright 2016 Nature Publishing Group.

graphene, followed by selectively attaching a secondary Pt atom to the preliminary one. The type of surface nucleation sites, selective deposition, the self-limiting nature of ALD, and the high stability of Pt single atoms all played a key role for successful preparation of the Pt₂ dimers. STEM images, X-ray absorption spectroscopy, and theoretical calculations suggest that the Pt₂ dimers are in the oxidized form of Pt₂O_x. The as-prepared graphene supported Pt₂ dimers exhibit much better activity than graphene supported Pt single atoms and Pt nanoparticles towards hydrolysis of ammonia borane for hydrogen generation. With the formation of Pt₂ dimers on graphene, the adsorption energies of both ammonia borane and H₂ molecules significantly decreased, which is the major reason for the high activity.

3.2.4 Galvanic replacement with substrates. The Pt single atoms are very active and mobile due to their extremely high surface energy, causing agglomeration during the preparation process. As a result, the Pt loading of Pt single atom catalysts is usually very low on substrates. The development of an effective method to achieve high loading of Pt SACs is still a great challenge for their future commercial application. As the support plays an important role in determining the interaction between Pt and substrates, the selectivity of substrates is also important for the dispersion of single atoms.

For example, Zeng and co-workers selected MoS₂ for the dispersion of Pt single atoms. They obtained Pt monomers on MoS₂ with a Pt mass loading of 7.5% (Fig. 14). The Pt/MoS₂

catalysts were synthesized by injecting K₂PtCl₆ solution into a solution containing MoS₂ nanosheets *via* a syringe pump, with the introduced Pt atoms replacing the Mo atoms in the nanosheets (Fig. 10C).¹⁴² The Pt mass loading (1.0%, 5.0% and 7.5%) can be precisely controlled by tuning the concentration and amount of K₂PtCl₆ solution (Fig. 12A–F). They found that the 7.5% Pt/MoS₂ catalysts contained a high ratio of neighbouring Pt monomers (Fig. 12I), which have lower energy barriers compared to isolated Pt single atoms; this results in more active CO₂ hydrogenation.

3.2.5 Photochemical reduction method. During a photochemical reduction process the atomic dispersion and separation, as well as the isolation of precursors on the substrates is vital. Secondly, to avoid the migration and agglomeration of Pt single atoms, the reaction phase is usually solid during the ultraviolet (UV) light treatment. For instance, Wang and Liu fabricated well-defined Pt single atoms on nitrogen-doped porous carbon (NPC) through a photochemical solid-phase synthesis (Fig. 15A). The PtCl₆²⁻ was adsorbed on the NPC support, followed by a UV light treatment (Fig. 15B and C). The loading amount of Pt can reach 3.8 wt%. The formation of pyridine-type Pt–N₄ coordination in the catalyst stabilized Pt single atoms, and it also serves as the active site for HER and ORR electrocatalysis.¹⁴³

Wu and co-workers demonstrated a facile approach to generate Pt single atoms on various substrates, including mesoporous carbon, graphene, carbon nanotubes, TiO₂ nanoparticles and ZnO nanowires, *via* photochemical reduction of

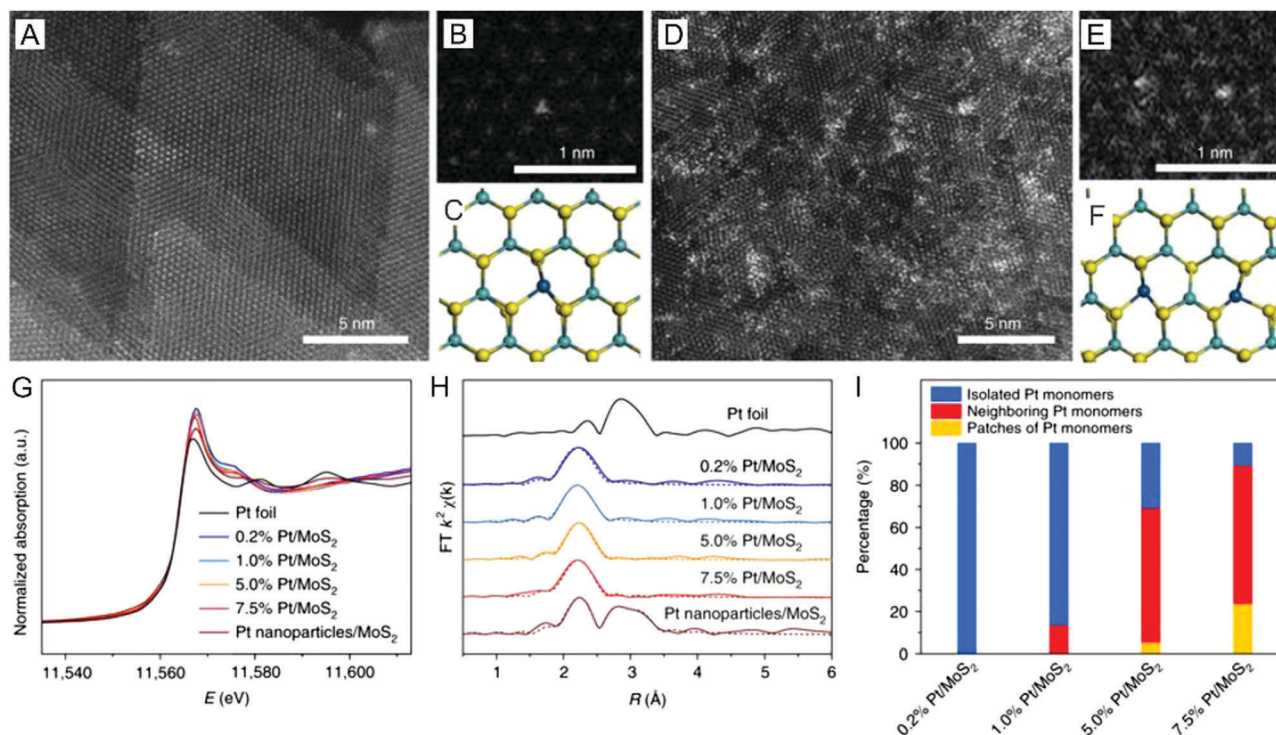


Fig. 14 (A–C) HAADF-STEM image and structural model of 0.2% Pt/MoS₂. (D–F) HAADF-STEM image and structural model of 7.5% Pt/MoS₂. (G and H) Pt K-edge X-ray absorption near edge spectra and K-edge EXAFS in R space for atomically dispersed Pt/MoS₂ and Pt nanoparticles/MoS₂. (I) Histogram of the contents of isolated Pt monomers, neighbouring Pt monomers, and patches of Pt monomers for atomically dispersed Pt/MoS₂ with different Pt loadings. Adapted with permission from ref. 142. Copyright 2018 Nature Publishing Group.

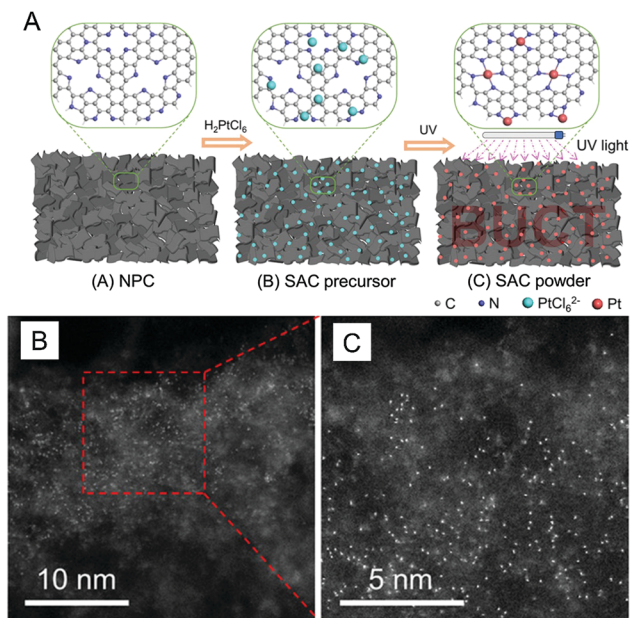


Fig. 15 (A) Schematic illustration of the photochemical formation of the Pt single atom/NPC catalyst. (B and C) HAADF-STEM images of the Pt single atom/NPC catalyst. Adapted with permission from ref. 143. Copyright 2018 American Chemical Society.

frozen H_2PtCl_6 solutions using UV light.¹⁴⁴ They found that the traditional UV irradiation of H_2PtCl_6 aqueous solutions produced 2 nm Pt crystals. Interestingly, the iced- H_2PtCl_6 aqueous solutions led to high density areas of isolated Pt atoms during the photochemical reduction process (Fig. 10E). The related DFT calculation results indicated that the formation of Pt single atoms in solution is an essential step for the fabrication of Pt single atoms on various substrates.

3.2.6 Spatial confinement strategy. The spatial confinement strategy was considered as an effective route to fabricate and stabilize single atom catalysts. Spatial confinement can be achieved by separating and encapsulating suitable mononuclear metal precursors with the aid of porous materials, such as zeolites, MOFs, *etc.* For example, the $[\text{Pt}(\text{NH}_3)_4]^{2+}$ complex can be confined by the molecular-scale pores of the KLTL zeolite. Then, the $\text{Pt}(\text{NH}_3)_4^{2+}/\text{KLTL}$ zeolite was oxidized at 633 K to obtain a well-defined Pt single atom catalyst.¹⁴⁵ Corma and co-workers prepared Pt single atoms and clusters in the MCM-22 structure. The Pt species were entrapped in the cups and cages during transformation from the two-dimensional into the three-dimensional MCM-22 zeolite.¹⁴⁶

Li and co-workers reported that noble metal nanoparticles (Pt, Pd and Au) can be transformed into well-dispersed stable single atoms at above 900 °C in an inert atmosphere on a ZIF-8 support.¹⁴⁷ They firstly prepared Pt nanoparticles on ZIF-8 nanocrystals to form Pt@ZIF-8 composites. Then the Pt@ZIF-8 nanocomposites were heated at 900 °C for 3 h to obtain Pt single atoms. The whole transformation process was systematically investigated on Pd@ZIF-8 composites. The particles grew bigger due to disorderly movement and intensive collisions within the supports at the initial stage; then the

size of particles decreased again through collision and coordination of surface metal atoms with the derived CN support (Fig. 10F). Density functional theory calculations revealed that the formation of single atoms at high-temperature was driven by the formation of the more thermodynamically stable noble metal- N_4 structure.

In addition to porous materials, two-dimensional materials were also effective supports to achieve spatial confinement of Pt species. Recently, Wang and co-workers synthesized partly charged Pt single atoms on anatase TiO_2 *via* an electrostatic-induction ion exchange and two dimensional confinement strategy (Fig. 16A).¹⁴⁸ The $[\text{Pt}(\text{NH}_3)_4]^{2+}$ complex intercalated into the interlayers of $\text{Na}_x\text{H}_{2-x}\text{Ti}_3\text{O}_7$ ($x = 0.75$) nanotubes through ion exchange with interlayered ions Na^+ . Then the Pt single atoms on TiO_2 were obtained by calcination at 400 °C, followed by treatment at 160 °C in a 5% H_2/N_2 atmosphere (Fig. 16B and C). The partially charged Pt single atoms on anatase TiO_2 exhibited better activity, optimal selectivity and excellent reusability toward anti-Markovnikov alkene hydrosilylation compared to commercial Pt/C.

3.3 Pt-Based single atom alloy catalysts

When Pt single atoms are deposited on metal substrates, they might exhibit some specific physical and chemical properties (such as catalysis) due to the formation of alloy structures. The as-prepared catalysts are referred to as single atom alloys. It should be emphasized that single atom alloys are not bimetallic dimers of two different single atoms alloyed together. The creation of Pt-based single-atom alloys is based upon deposition of Pt single atoms on another host metal surface.

Flytzani-Stephanopoulos and Sykes prepared Pt single atoms on a clean Cu(111) surface using physical vapour deposition held at 380 K.^{149,150} Scanning tunnelling microscopy images clearly showed that Pt atoms incorporate both directly into Cu(111) terraces and in areas above surface step edges *via* place exchange. Alternatively, single atom alloy catalysts can be obtained through a galvanic replacement reaction.^{151,152} Firstly, Cu nanoparticle catalysts were synthesized by immobilizing polyvinylpyrrolidone-stabilized copper nanoparticles onto a silica support followed by calcination at 300 °C in air. Then the Pt single atoms were deposited onto Cu particles by galvanic replacement. The Pt to Cu ratio can be tuned by controlling the amount of Pt precursor. The as-prepared Pt-Cu single atom alloy catalysts exhibited distinct catalytic performance in several reactions, such as selective hydrogenation of 1,3-butadiene, CO adsorption, selective formic acid dehydrogenation and C-H activation reactions, compared to traditional Pt catalysts.

Although Pt single atom alloy catalysts have been successfully prepared through physical vapour deposition and galvanic replacement reactions, they are rarely applied in electrochemical catalytic reactions. Hence, the rational design of Pt single atom alloys with multiple compositions should be explored in the future, as bimetallic catalysts can exhibit improved performance compared to the pure metals for electrocatalytic reduction.

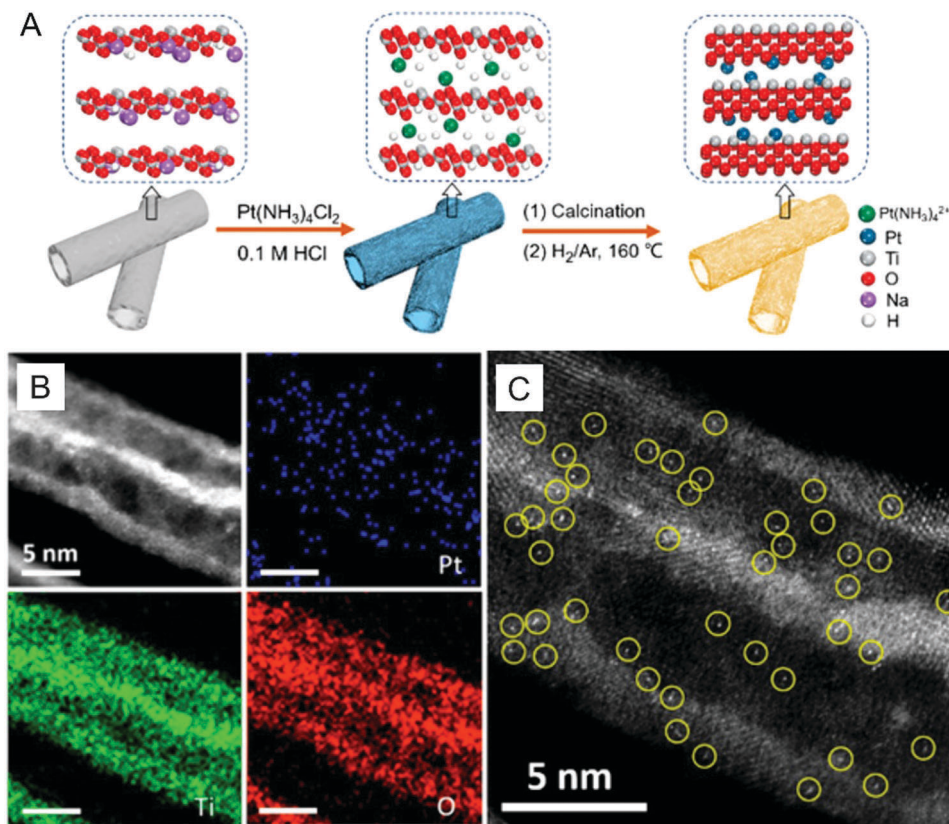


Fig. 16 (A) Schematic illustration of the formation of the partially charged Pt single atom/TiO₂ catalyst via an electrostatic-induction ion exchange and two dimensional confinement strategy. (B and C) HAADF-STEM-EDS element mapping and HAADF-STEM images of the Pt single atom/TiO₂ catalyst. Adapted with permission from ref. 148. Copyright 2018 American Chemical Society.

3.4 Strategies for improving the stability of Pt single atom catalysts

Due to the high surface energy of single atom catalysts, the Pt atoms tend to diffuse and aggregate on the support during the catalytic reactions. Atom trapping is an applicable way for protecting single atom catalysts. The strong interaction between Pt and the support plays an important role in enhancing the stability of single atoms. It has been reported that the N atoms on a substrate such as N-doped carbon black, N-doped graphene and TiN can effectively anchor Pt single atoms. Thanks to the formation of Pt–N bonding, the single atom catalysts not only exhibited good stability, but also much improved catalytic properties. Besides, several metal oxides are known to influence heterogeneous catalyst stability through strong metal–support interactions. For example, Datyel *et al.* found that when Pt/Al₂O₃ was mixed with CeO₂ rods, the Pt atoms transferred to the ceria forming an atomically dispersed catalyst.¹²⁹ With the deposition of Pt on well-controlled CeO₂, ceria helped to trap atomically dispersed Pt, meanwhile the strong interaction between Pt and ceria also helped preserve the surface area of polyhedral ceria.

To stabilize Pt nanoparticles on a support, Flytzani-Stephanopoulos and co-workers used small amounts of alkali ions (sodium or potassium) to modify the Pt catalysts on alumina or silica.¹⁵³ The subnanometer Pt clusters and atoms present on

the Na-modified silica surfaces were stable after several heat treatments in air at 400 °C. Both experimental evidence and DFT calculations suggest that a partially oxidized Pt–alkali–O_x(OH)_y species is the active site for the low-temperature Pt-catalyzed WGS reaction. To further understand the enhanced mechanism, Flytzani-Stephanopoulos *et al.* recently created Pt–Na_x–O_y–(OH)_z clusters by co-impregnation of Pt and Na onto a 1000 °C-annealed MWNT surface (Fig. 17A).¹⁵⁴ The atomically dispersed platinum species are stabilized by the addition of sodium. These subnanometer-sized active sites improve the water–gas shift activity to levels comparable to those obtained with highly active Pt catalysts on metal oxide supports. *In situ* atmospheric pressure X-ray photoelectron spectroscopy (AP-XPS) experiments demonstrated that oxidized platinum Pt–OH_x contributions in the Pt 4f signal are higher in the presence of sodium. This result provided evidence for a previously reported active-site structure of the form Pt–Na_x–O_y–(OH)_z. By binding Pt to sodium ions through –O ligands, they can obtain single-atom-centric Pt sites on TiO₂, 1-zeolites, and mesoporous silica MCM-41 (Fig. 17B–D).¹⁵⁵ The single-atom-centric Pt sites stabilized by sodium through –O ligands are active and stable in realistic WGS reaction mixtures from ~120 to 400 °C. These results also reveal that the properties are invariant to the choice of the support.

In addition to the creation of strong interactions between Pt and the support, encapsulation is another effective strategy for

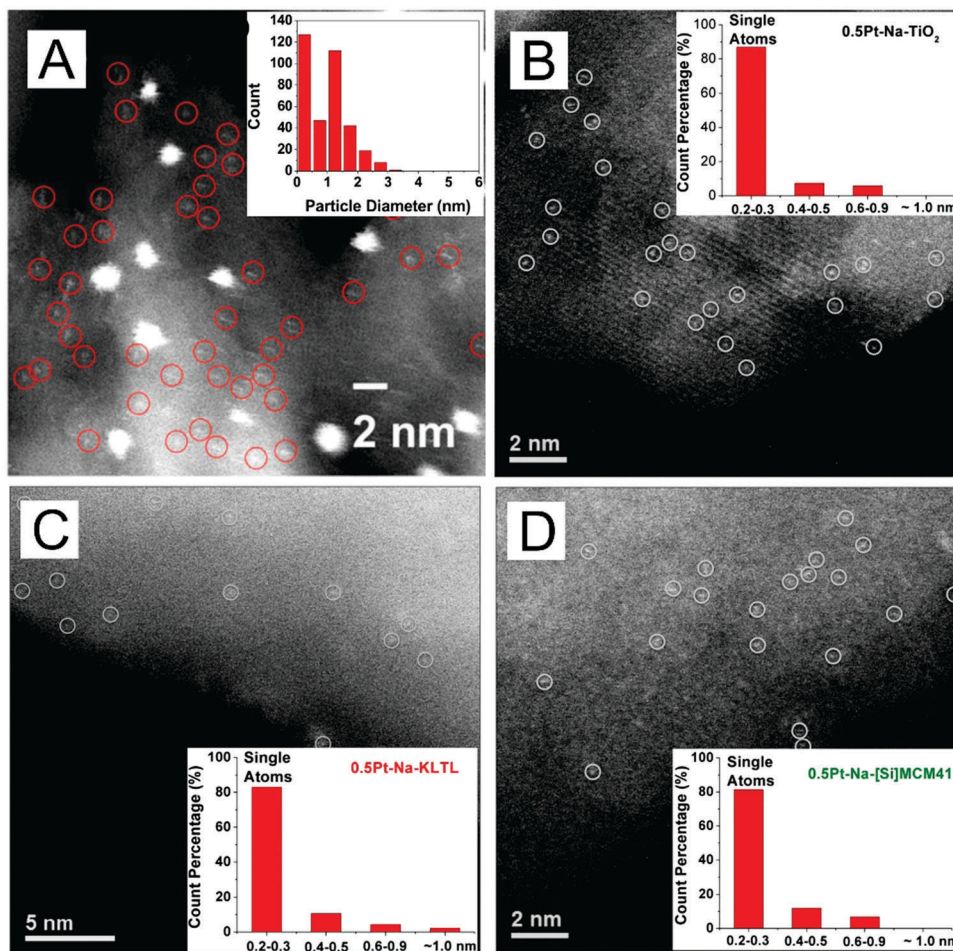


Fig. 17 (A) HAADF-STEM images of 1 wt% Pt₁Na₆ on carbon multiwalled carbon nanotubes after use in the WGS reaction. Adapted with permission from ref. 154. Copyright 2014 American Chemical Society. (B–D) HAADF-STEM images of Na-containing Pt single atom catalysts on (B) TiO₂, (C) L-zeolites, and (D) mesoporous silica MCM-41. Adapted with permission from ref. 155. Copyright 2015 American Chemical Society.

stabilizing single atom catalysts. Because of their microporous cavities/channels and high thermal stability, zeolite materials appear to be promising supports for preparing encapsulated single atom catalysts. Gate and co-workers encapsulated Pt single atoms in zeolite KLTL by mixing zeolite KLTL and aqueous [Pt(NH₃)₄](NO₃)₂, followed by oxidizing the mixture at 633 K.¹⁴⁵ The Pt single atoms maintained isolated sites after the oxidation and catalytic CO oxidation reactions. Recently, Corma *et al.* presented a new strategy for encapsulating Pt single atoms and clusters with MCM-22 during its transformation process from two-dimensional into three-dimensional structures.¹⁴⁶ Pt atoms are incorporated into the cups and cages of the MCM-22 zeolite, exhibiting exceptionally high stability. The Pt single atoms and clusters maintained their size after calcination in air at 650 °C. The ALD deposition of metal oxide around Pt catalysts has been proven as another effective way to encapsulate Pt clusters (Fig. 18A). Sun *et al.* developed a facile approach to encapsulate Pt atoms in ZrO₂ nanocages by area-selective ALD.¹³⁰ By using oleylamine as the blocking agent, ALD ZrO₂ was selectively deposited around Pt atoms, which avoided the diffusion and aggregation of Pt atoms

(Fig. 18B–D). For the ORR performance, the ZrO₂-protected Pt catalysts showed nine and ten times more stability than ALDPT/NCNT and Pt/C catalysts, respectively.

4. Electrochemical applications of Pt-based catalysts with high AUE

4.1 Oxygen reduction reaction

Until now, the commercial cathode catalysts in proton-exchange membrane fuel cells are still Pt-based nanoparticles, due to their excellent performance for the ORR. According to a 2012 report from the Department of Energy, the Pt loading in a PEMFC must be reduced by at least 4-fold to meet the cost requirement for widespread commercialization.¹⁵⁶ In addition, the mass activity for the U.S. Department of Energy's 2017 target is 0.44 A mg_{Pt}⁻¹. With the increase of the AUE of Pt-based catalysts, the ORR performance can be greatly enhanced and meet the Department of Energy's target.

The particle size is a significant factor in the ORR performance of Pt catalysts. Due to the various types of electrolyte, the

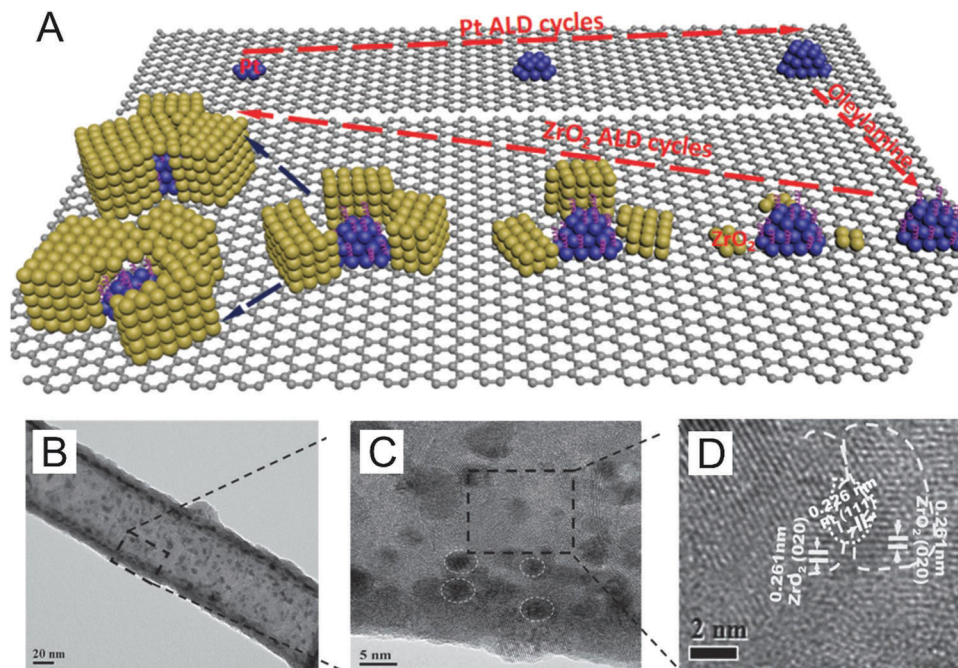


Fig. 18 (A) Schematic diagram of Pt encapsulated in ZrO_2 nanocage structures fabricated by area-selective ALD. (B–D) HRTEM images of ALD ZrO_2 -Pt/NCNT catalysts with 50 cycles of ALD ZrO_2 . Adapted with permission from ref. 130. Copyright 2015 Wiley-VCH.

different types of Pt catalysts and various testing conditions, the relationship between the mass activity and particle size is not consistent in the references. For instance, Shao and Peles showed that 2.2 nm Pt nanoparticles exhibited a mass activity of $0.11 \text{ A mg}_{\text{Pt}}^{-1}$, the best amongst the Pt particles ranging in size from 1–5 nm.¹¹⁷ Shao-Horn found that the mass activity increased from 0.07 to $0.3 \text{ A mg}_{\text{Pt}}^{-1}$, with the size decreasing from 4.7 nm to 1.7 nm.¹¹⁹ When the particle size is decreased to the single atom scale, the peroxide reduction reaction would be suppressed due to the site-blocking spectator species and low Pt-content. As a result, H_2O_2 would be yielded instead of H_2O .^{126,135} For example, Pt-Hg/C nanoparticles with isolated Pt atoms on the surfaces exhibited a selectivity of hydrogen peroxide up to 96% and a mass activity of $26 \text{ A g}_{\text{noble metal}}^{-1}$ at a 50 mV overpotential.¹⁵⁷ As shown in Fig. 19A and B, Pt/HSC catalyses the ORR reaction predominately through a two-electron pathway ($n = 2.1$).¹²⁶ When the reaction is carried out in an electrochemical H-cell, Pt/HSC showed a $97.5 \text{ mmol h}^{-1} \text{ cm}^{-2}$ H_2O_2 production rate during the initial 1 h. It should be pointed out that the support plays a significant role for the performance of single atom catalysts. Soon and Lee prepared single-atom Pt catalysts on TiC and TiN supports. The Pt/TiC catalyst showed much better activity and stability for the reduction of O_2 to H_2O_2 .¹⁵⁸ DFT calculation results indicated that the oxygen species have stronger bonding to Pt/TiN; while the Pt/TiC surface could promote oxygen–oxygen bonding, which resulted in higher selectivity for H_2O_2 production. What is more, the support can even determine the ORR route. When single atoms were deposited on N-doped carbon black, they exhibited great ORR performance.¹³⁷ DFT calculations indicate that the single-pyridinic-nitrogen (P-N)-atom-anchored Pt single

atom centres are the main active sites, which are highly active for the ORR.

Well-controlled Pt nanostructures exhibit much better mass activity than the smaller sized particles. The cubic Pd@Pt core-shell nanocrystals with 2–3 Pt atomic layers exhibited a mass activity of 0.24 A mg^{-1} at 0.9 V (normalized by Pt), combined with a good stability after 10 000 cycles.⁸¹ DFT results showed that the binding of OH to $\text{Pt}_{\text{hL}}^*/\text{Pd}(100)$ surfaces was weaker than pure Pt nanocubes, which promoted OH hydrogenation during the ORR. Compared to the cubic structures with {100} facets, octahedral Pd@Pt core-shell catalysts showed a mass activity of 0.49 A mg^{-1} at 0.9 V (normalized by Pt), which is almost two times larger than cubic core-shell surfaces.⁸⁶ Furthermore, with the formation of Pd@Pt icosahedral core-shell structures, the Pt layers are forced into a compressed, corrugated structure, due to the tensile strain of the five-fold twinned Pd seeds.⁸⁹ DFT calculation results indicated that the compressive strain imposed on the Pt overlayers, together with the core-shell structure, weakened the binding strength of reaction intermediates. As a result, the mass activity of Pd@Pt_{2.7L} icosahedra was measured to be 0.64 A mg^{-1} at 0.9 V (normalized by Pt), 7.2 times higher than that of traditional Pt/C catalysts.⁸⁹ Xia *et al.* also tried to overgrow Pt on Pd decahedra with twin defects. Due to the strong adsorption of Pt adatoms on edge/ridge sites, the obtained Pd@Pt core-shell decahedra exhibited a concave structure.⁹¹ The concave structure provided a positive effect for enhancing the specific activity (normalized by the ECSA) of the catalysts. Together with the high AUE, ligand effect and strain effect arising from the lattice mismatch between Pd and Pt, the mass activity of concave Pd@Pt core-shell decahedra reached 1.6 A mg^{-1} at 0.9 V (normalized by Pt). After 10 000 cycles, the

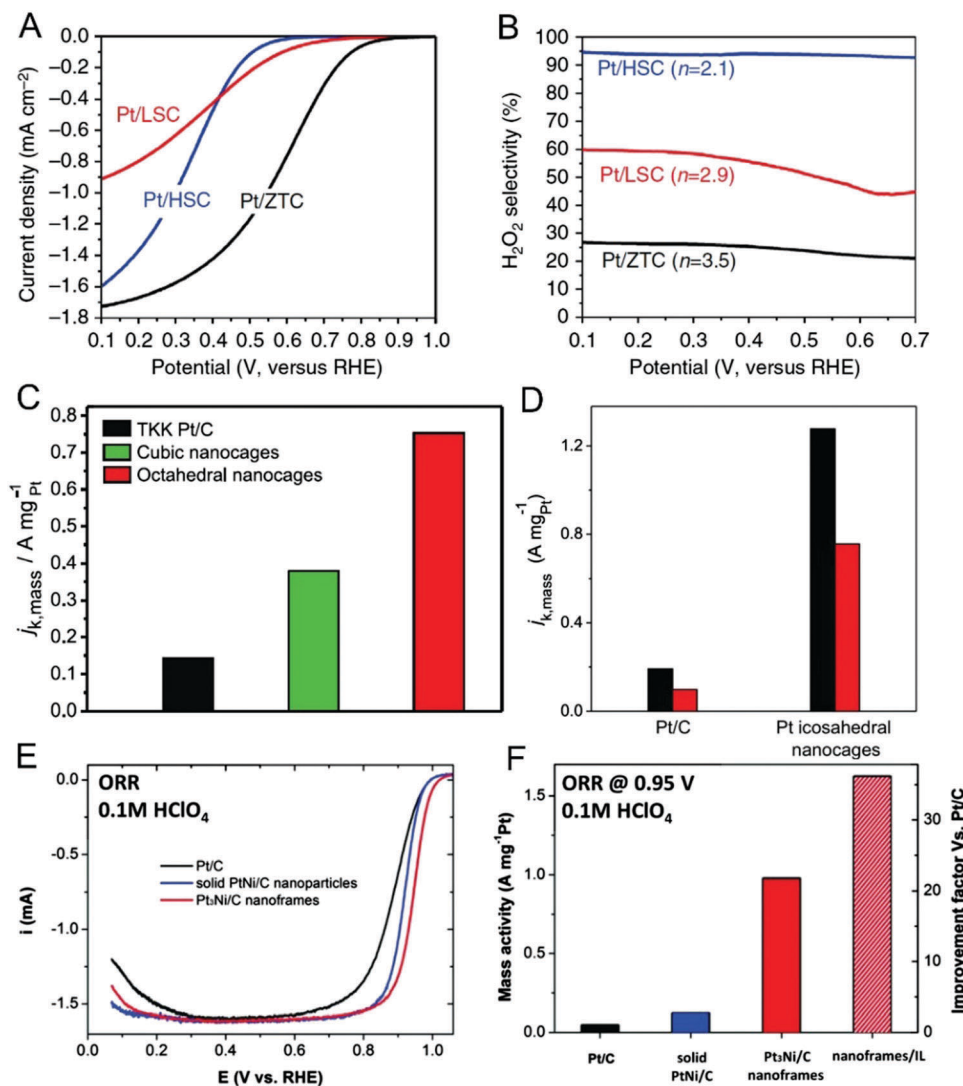


Fig. 19 (A) ORR activities of the Pt single atom catalysts on LSC, HSC and ZTC supports (ZTC: zeolite-templated carbon, LSC: low S-content ZTC, HSC: high S-content ZTC). (B) H₂O₂ production selectivity. Adapted with permission from ref. 126. Copyright 2016 Nature Publishing Group. (C and D) Comparison of the ECSAs and mass activities for the carbon-supported Pt nanocages and the commercial Pt/C catalyst. Adapted with permission from ref. 96 (Copyright 2015 American Association for the Advancement of Science), and 97 (Copyright 2016 American Chemical Society). (E) ORR polarization curves of Pt/C and Pt₃Ni/C catalysts. (F) Mass activities of Pt/C and Pt₃Ni/C catalysts measured at 0.95 V, and improvement factors versus Pt/C catalysts. Adapted with permission from ref. 104. Copyright 2014 American Association for the Advancement of Science.

mass activity decreased to 0.69 A mg⁻¹ at 0.9 V (normalized by Pt), still a marked improvement over other core-shell catalysts. It should be mentioned that, for Pd@Pt core-shell structures, when the mass activity is normalized by the total amount of noble metal (Pd + Pt), the mass activity decreases significantly. For example, the mass activity of octahedral Pd@Pt catalysts (normalized by Pd + Pt) is approximately 0.15 A mg⁻¹, much smaller than the Pt normalized mass activity of 0.49 A mg⁻¹.⁸⁶ To further increase the mass activity of the core-shell structures, the selective etching of Pd cores would fabricate nanocage structures, which could provide interior atom active sites for the ORR. Based on this point, cubic, octahedral and icosahedral nanocages are fabricated through a selective etching method. Thanks to the additional active sites provided by the interior walls, the nanocage structures exhibited two times higher mass activity than core-shell structures.

Specifically, the mass activity for cubic, octahedral and icosahedral nanocages was 0.38, 0.75 and 1.28 A mg⁻¹ at 0.9 V as shown in Fig. 19C and D.^{96–98}

As Ni can reduce the d-band of Pt atoms, the activity for PtNi is much higher than pure Pt. With the combination of high AUE and multi-composition, the ORR activity for Pt-based catalysts can be further increased. For example, Pt₃Ni nanoframes exhibited a mass activity of 5.7 A mg⁻¹ at 0.9 V, which is more than an order of magnitude greater than the U.S. Department of Energy's 2017 target (Fig. 19E and F).¹⁰⁴ In addition, the Pt₃Ni nanoframes showed remarkable durability for a duration of 10 000 cycles. The Pt-skin surfaces lowered the coverage of oxygenated intermediates and protected the subsurface transition metal from electrochemical corrosion. PtNiCo nanowires with a diameter of 4–5 atomic layers

demonstrate a mass activity of 4.20 A mg^{-1} at 0.9 V .⁶⁶ Furthermore, the as-prepared ultra-thin alloy nanowires are very stable with negligible activity decay over the course of 30 000 cycles.

4.2 Methanol and formic acid oxidation reactions

In direct methanol fuel cells and direct formic acid fuel cells, the most expensive component is the Pt-based catalysts. As the whole fuel cell system contains several parameters, it is necessary to develop a facile reaction system to estimate the activity of Pt catalysts. Therefore, methanol and formic acid electrochemical oxidation are employed as the references to determine the performance of the catalysts.

According to the catalytic mechanism model for the methanol oxidation reaction (MOR) on a Pt surface, three Pt atoms are required to fabricate an active site for the MOR.¹⁵⁹ As a result, Pt single atoms did not show any activity. With the formation of Pt clusters, activity for the MOR appears and the onset potential decreased with the decrease of cluster size.¹³¹ Pt nanowire structures also exhibited great performance for the MOR. As shown in Fig. 20A and B, the specific and mass electrocatalytic activities of ultrathin nanowires were recorded at 2.48 and 1.74 times those of the commercial Pt/C electrocatalyst for methanol oxidation.⁶³ Moreover, PtRuM (M = Ni, Co and W) alloy nanowires were fabricated for improving the activity for the MOR. The Pt₇Ru₂Fe nanowire catalysts exhibited a specific activity of 1.10 mA cm^{-2}

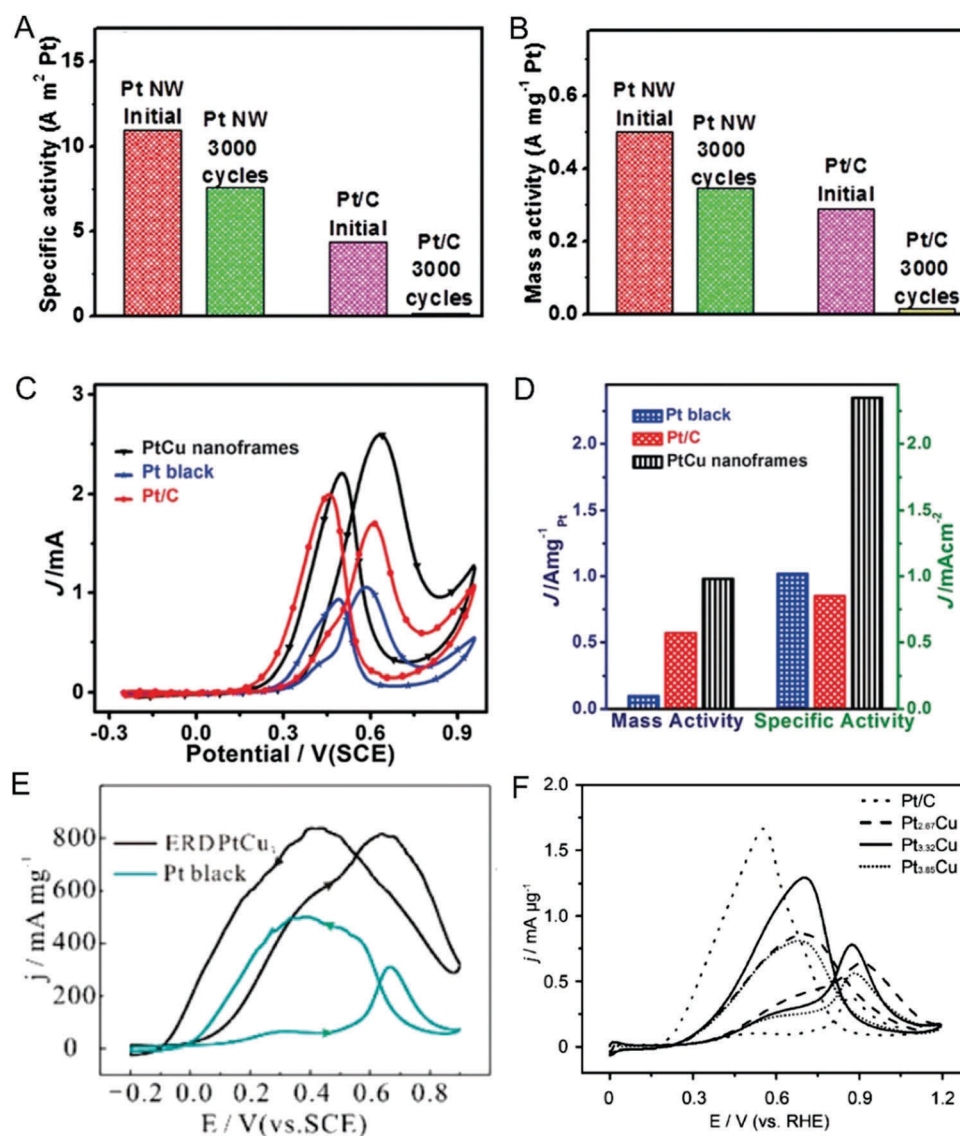


Fig. 20 (A and B) Comparative specific and mass activity for methanol oxidation before and after 3000 cycles of Pt nanowires and commercial Pt/C electrocatalysts. Adapted with permission from ref. 63. Copyright 2013 American Chemical Society. (C) Methanol electrooxidation curves of rhombic dodecahedral PtCu nanoframes, commercial Pt/C and Pt black catalysts. (D) Specific activity (normalized by the ECSA) and mass activity of rhombic dodecahedral PtCu nanoframes. Adapted with permission from ref. 110. Copyright 2015 Wiley-VCH. (E) The mass activities of ERD PtCu₃ alloy NCs and commercial Pt for the formic acid oxidation reaction. Adapted with permission from ref. 109. Copyright 2015 American Chemical Society. (F) Mass activities of Pt–Cu HTBNFs with different Pt/Cu ratios for formic acid oxidation. Adapted with permission from ref. 111. Copyright 2015 Wiley-VCH.

(normalized by the ECSA), better than that of nanowires with other compositions.⁶² With the introduction of Ru in Pt, the onset potential decreased due to the formation of Ru–OH species. The presence of Fe lowered the d-band center of Pt and thereby altered the electronic properties of the overall alloy. In addition, Pt–Cu alloy nanoframes are another effective catalyst for the MOR. Huang and co-workers reported that rhombic dodecahedral PtCu nanoframes have a mass activity of 0.98 A mg⁻¹ at 0.63 V, which is 1.72 and 10.1 times greater than the mass activities of commercial Pt/C (0.57 A mg_{Pt}⁻¹) and Pt black catalysts (0.097 A mg_{Pt}⁻¹), respectively (Fig. 20C and D).¹¹⁰

The formic acid oxidation reaction is another potential anode fuel cell reaction which has attracted increased attention. For excavated rhombic dodecahedral (ERD) PtCu₃ alloy NCs, the mass activity for formic acid oxidation at 0.65 V in the forward potential scan is 0.815 A mg⁻¹, which is much higher than that of commercial Pt black (Fig. 20E).¹⁰⁹ For formic acid oxidation, the ratio of the forward oxidation current density peak (j_f) to the reverse peak (j_b) (i.e., j_f/j_b) reflects the catalyst tolerance. The j_f/j_b ratio of ERD PtCu₃ alloy NCs is in the range from 0.85 to 0.95, indicating high antipoisoning ability for these catalysts. Pt–Cu HTBNFs with different Pt/Cu ratios also exhibited good activity for formic acid oxidation. The mass activities of Pt_{2.67}Cu (0.64 A mg_{Pt}⁻¹), Pt_{3.32}Cu (0.78 A mg_{Pt}⁻¹), and Pt_{3.85}Cu (0.56 A mg_{Pt}⁻¹) HTBNFs are 1.7, 2.1, and 1.5 times larger than Pt/C, respectively (Fig. 20F).¹¹¹ Although the ECSAs of the Pt catalysts are smaller than commercial Pt/C, the improvement of mass activity is attributed to synergetic effects between Pt and Cu. In addition, the j_f/j_b ratios are approximately 0.7, which is much higher than 0.23 for Pt/C, indicating good durability.

4.3 Hydrogen evolution reaction

Hydrogen is a clean energy carrier, as the by-product is only water. As a result, hydrogen is believed to be one of the most promising energy sources, and can be applied in novel-energy areas. Currently, the main route for hydrogen production is through steam-reformed methane, sourced from fossil fuel reserves, with a substantial amount of CO₂ being generated during the reaction. Therefore, the development of environmentally friendly routes for hydrogen production remains a great challenge. Water electrolysis is one promising alternative route to generate hydrogen; however, the sluggish kinetics of the HER causes high overpotentials and an associated large energy consumption, which greatly hinder the practical application of electrochemical production of hydrogen. The HER activity is greatly dependent on the heterogeneous catalysts on the working electrode. In the HER test, parameters including the onset potential, current density (specific activity and mass activity), overpotential at 10 mA cm⁻², Faradaic efficiency, Tafel slope and durability are usually measured to evaluate the electrocatalytic efficiency.¹⁶⁰ Up till now, Pt is considered the most effective electrocatalyst for the HER. Nevertheless, increasing the mass activity of Pt is always the ultimate goal for electrocatalysts designed to achieve cost-effective hydrogen production.

Xiong *et al.* prepared a Pd@Pt core–shell structure with ultra-thin Pt shells on graphene, which reached the 10 mA cm⁻² metric at an overpotential of around 15 mV.⁸³ DFT results showed that distinct interfacial polarization occurs when the Pt atoms are 1–2 atomic layers thick, resulting in substantial negative charges. The increase in electron density on the Pt shell surface is responsible for the enhanced HER activity. In addition, simulations reveal that the graphene support can facilitate charge transfer and ionic interchange to enhance the activity for the HER.

In addition to core–shell structures, Pt single atom catalysts exhibited extremely high mass activity for the HER due to their high AUE of almost 100% (Fig. 21A). It is found that the specific activity (normalized by the area of a glassy carbon rotating-disk electrode) of Pt single atoms on NGNs was only around 2 times larger than commercial Pt/C.¹²⁸ When normalized to the Pt loading, the mass activity of the HER for the ALD50Pt/NGN catalysts at an overpotential of 0.05 V was 10.1 A mg⁻¹, 37.4 times greater than the Pt/C catalyst (Fig. 21B). Thanks to the strong bonding energy between Pt and nitrogen doped graphene, the activity of ALD50Pt/NGN catalysts dropped only 4% at an overpotential of 0.05 V after 1000 cycles (Fig. 21C and D). In addition, a smaller Tafel slope, 29 mV dec⁻¹, was obtained in comparison to the 31 mV dec⁻¹ of Pt/C catalysts further demonstrating the increased HER progress. The Pt single atoms on the N-doped graphene contain more unoccupied 5d orbitals. During the HER process, the 5d orbitals of the Pt atoms interact strongly with the 1s orbital of the H atoms, leading to electron pairing and hydride formation. Aside from the N-doped graphene support, SL-Ni(OH)₂ was found to be an effective support for enhancing Pt based catalysts. A Pt nanowire/SL-Ni(OH)₂ catalyst exhibited a specific activity (normalized by the ECSA) of 2.48 mA cm⁻² and a mass activity of 1.59 A mg⁻¹ at an overpotential of 0.07 V in 1 M KOH solution, 9 and 4.5 times larger than that of commercial Pt/C, respectively.⁶⁹ The activation of the HO–H bond by Ni(OH)₂ and the active sites of Pt nanowires are responsible for the enhanced HER activity. Furthermore, Pt nanowire/SL-Ni(OH)₂ keeps 95.7 and 98.3% of its initial activity in 1 and 0.1 M KOH after 11 hours. As a comparison, without the combination of SL-Ni(OH)₂, pure Pt nanowires only maintain 61.6 and 79.0% of their initial activity in 1 and 0.1 M KOH after 11 hours, indicating the stabilizing influence of Ni(OH)₂ on the Pt nanowires. In addition, most of the Pt nanowires maintained their 1D ultrathin structure, aiding their superior durability.

5. Summary and outlook

Regarding nanostructured Pt-based catalysts, there is a strong correlation between their electrochemical mass activity (for the ORR, HER and MOR) and the atom utilization efficiency; as such, many studies focus on the development of synthetic strategies for Pt-based catalysts with high AUE. Most of the new achievements have been discussed in this review. For example, porous structures are usually fabricated through an

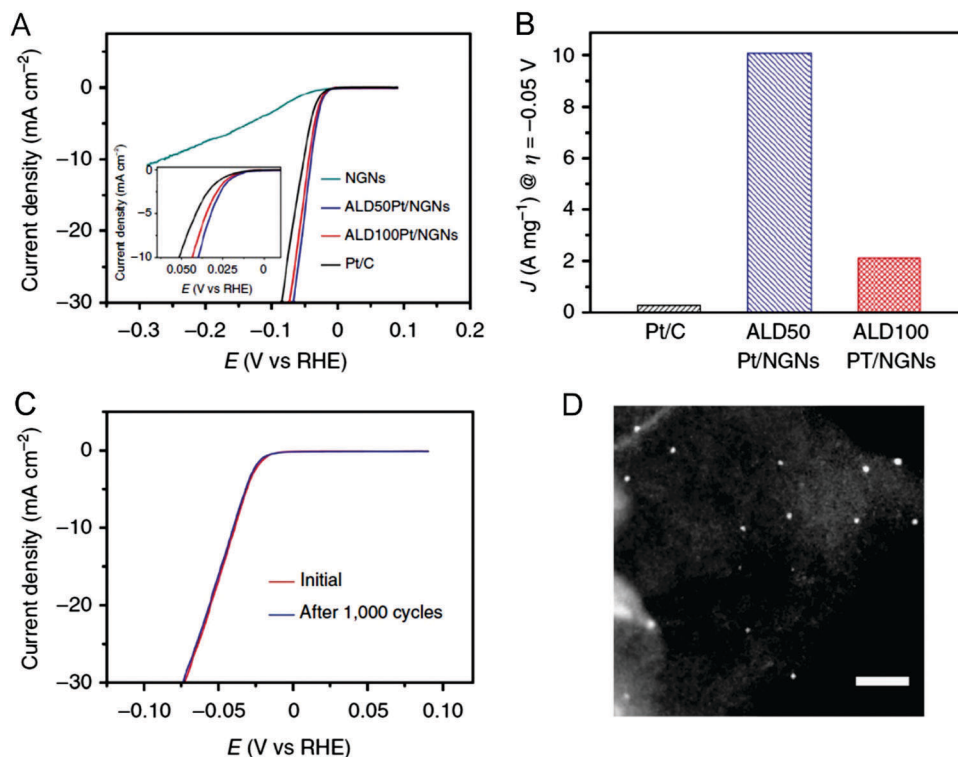


Fig. 21 Electrocatalytic properties. (A) The HER polarization curves for ALD Pt/NGN and Pt/C catalysts. The inset shows the enlarged curves at the onset potential region of the HER for the different catalysts. (B) Mass activity at 0.05 V (*versus* RHE) of the ALD Pt/NGN and the Pt/C catalysts for the HER. (C) Durability measurement of the ALD 50Pt/NGN. (D) STEM images of ALD 50Pt/NGN samples after durability testing. Adapted with permission from ref. 128. Copyright 2016 Nature Publishing Group.

oriented attachment mechanism. Ultra-thin nanowires also have a high Pt AUE due to their extremely thin diameter and high length-diameter ratio. Well-controlled core-shell structures can be obtained through galvanic replacement of Cu and direct deposition onto Pd substrates. During the direct growth process, the formation of ultra-thin uniform Pt shells is highly determined by the deposition rate and diffusion rate. In addition, ultrathin nanocages can be prepared from core-shell structures through a selective etching method. It should be mentioned that the relationship between mass activity and AUE cannot be applied in all catalytic reactions, as the catalytic reaction route might be tuned with the transformation from nanoparticles to clusters and single atoms. For example, Pt single atoms may not be an effective catalyst for the reduction of O₂ to H₂O. With a decrease in particle size, Pt single atoms with an AUE of almost 100% can be obtained by co-precipitation, wet-impregnation and ALD methods. Although several synthetic strategies have been developed for the preparation of Pt catalysts with high AUE, more research should be directed to the following aspects:

(i) The synergistic effect between the high AUE, surface control and composition of nanostructured Pt catalysts. As previously mentioned, the performance of nanostructured Pt-based catalysts can be improved by tuning their AUE, surface structure and composition. However, most studies focus on one or two factors to improve the activity and durability of Pt-based catalysts. It is difficult to accomplish surface control and reduce

particle size at the same time, due to the ratio increase of edge/surface atoms with the decrease in particle size. The rational design of nanostructured Pt-based catalysts (nanowire, core-shell, and hollow structures) can combine a high AUE, a well-controlled surface structure and a multiple composition catalyst to offer more possibilities for further enhancing their mass activities.

(ii) The stability of single atom catalysts. As single atom catalysts are rich in low-coordination atoms, the surface energy is extremely high. The atoms are highly mobile and tend to aggregate during the catalytic reactions. It has been reported that the interaction between the metal atom and its support plays a critical role in their stability and activity. Several studies showed that single Pt atoms on nitrogen-doped carbon black, graphene and nitrogen-doped graphene can form strong coordination, thus exhibiting good stability during catalytic processes. In the future, it is of great importance to systematically understand the internal relationship between single atom coordination structures, the single atom-support interactions, and the support properties. In addition, more studies should focus on the development of effective stabilizers. For example, the selective deposition of metal oxide around Pt catalysts can protect Pt atoms from aggregation. The rational design of porous substrates to pin the Pt atoms in pores may also increase the stability of single atom catalysts.

(iii) The high loading of Pt in single atom catalysts. Although several different methods have been developed for the preparation

of Pt single atoms, the majority of reported Pt single atom catalysts are lower than 5 wt%. It is still a great challenge to achieve higher loading of Pt (10–20 wt%) on the support. Successful high single atom Pt loading could introduce single atom catalysts to more catalytic reactions and accelerate their applications in industrial areas.

(iv) Scaling up the synthesis. Currently, 1–5 nm Pt particles can be obtained through industrial production. However, the fabrication of Pt single atoms or well-controlled nanostructures remains exclusively at the laboratory-scale. The loading amount of Pt single atoms on supports is still very low, a hurdle for further commercial applications. As a result, it remains a great challenge to increase the loading amount of Pt single atom catalysts to the same level as commercial Pt/C catalysts. For well-controlled nanostructures, the uniformity of particle size and morphology would be reduced when simply increasing the reactant amount in the reaction system, due to the influence of heat and mass transfer during the process. Therefore, it remains a great challenge to scale up novel Pt-based catalysts with high AUE. Recently, continuous flow synthesis based on droplets provided a creative platform for the synthesis of well-controlled Pd and Ag nanoparticles, which is promising for the large scale production of well-controlled Pt-based catalysts.^{161,162}

(v) Applications in real industrial reaction systems. As we described in the review, most of the Pt-based catalysts were applied in the ORR and methanol/formic acid oxidation reaction to evaluate their electrochemical performance. To move from evaluation models to industrial applications, more studies should focus on the application of these catalysts in whole fuel cell systems, such as direct methanol fuel cells and proton exchange membrane fuel cells.

Although these recent advancements in the development of Pt-based catalysts with high AUE are still limited in terms of large-scale applications, they offer many solutions for optimizing the structures of the catalysts to meet the performance required in industry. Furthermore, a systematic study on the syntheses of Pt-based catalysts with high atom utilization efficiency would provide worthwhile insight for preparation of other noble metal NCs.

Conflicts of interest

There are no conflicts to declare.

Acknowledgements

This research was supported by the Natural Science and Engineering Research Council of Canada (NSERC), the Canada Research Chair Program (CRC), the Canada Foundation for Innovation (CFI), and the University of Western Ontario (UWO).

References

- 1 B. C. H. Steele and A. Heinzl, *Nature*, 2001, **414**, 345.
- 2 M. K. Debe, *Nature*, 2012, **486**, 43.
- 3 A. C. Chen and P. Holt-Hindle, *Chem. Rev.*, 2010, **110**, 3767.
- 4 M. Martins, C. Mourato, S. Sanches, J. P. Noronha, M. T. B. Crespo and I. A. C. Pereira, *Water Res.*, 2017, **108**, 160.
- 5 H. A. Gasteiger, S. S. Kocha, B. Sompalli and F. T. Wagner, *Appl. Catal., B*, 2005, **56**, 9.
- 6 X. Zhao, S. Chen, Z. Fang, J. Ding, W. Sang, Y. Wang, J. Zhao, Z. Peng and J. Zeng, *J. Am. Chem. Soc.*, 2015, **137**, 2804.
- 7 Y. Bing, H. Liu, L. Zhang, D. Ghosh and J. Zhang, *Chem. Soc. Rev.*, 2010, **39**, 2184.
- 8 L. Zhang, S. Yu, J. Zhang and J. Gong, *Chem. Sci.*, 2016, **7**, 3500.
- 9 T. Yoshida and K. Kojima, *Electrochem. Soc. Interface*, 2015, **24**, 45.
- 10 S. S. Munjewar, S. B. Thombre and R. K. Mallick, *Renewable Sustainable Energy Rev.*, 2017, **67**, 1087.
- 11 H. Liu, C. Song, L. Zhang, J. Zhang, H. Wang and D. P. Wilkinson, *J. Power Sources*, 2006, **155**, 95.
- 12 C. Rice, S. Ha, R. I. Masel and A. Wieckowski, *J. Power Sources*, 2003, **115**, 229.
- 13 C. Rice, S. Ha, R. I. Masel, P. Waszczuk, A. Wieckowski and T. Barnard, *J. Power Sources*, 2002, **111**, 83.
- 14 Z. M. Peng and H. Yang, *Nano Today*, 2009, **4**, 143.
- 15 J. Y. Chen, B. Lim, E. P. Lee and Y. Xia, *Nano Today*, 2009, **4**, 81.
- 16 A. C. Chen and P. Holt-Hindle, *Chem. Rev.*, 2010, **110**, 3767.
- 17 S. S. Cheong, J. D. Watt and R. D. Tilley, *Nanoscale*, 2010, **2**, 2045.
- 18 Z. Y. Zhou, N. Tian, J. T. Li, I. Broadwell and S. G. Sun, *Chem. Soc. Rev.*, 2011, **40**, 4167.
- 19 Z. Luo, C. Tan, Z. Lai, X. Zhang, J. Chen, Y. Chen, B. Chen, Y. Gong, Z. Zhang, X. Wu, B. Li, Y. Zong, L. Gu and H. Zhang, *Sci. China Mater.*, 2018, DOI: 10.1007/s40843-018-9315-5.
- 20 J. Zhang, H. Yang, J. Fang and S. Zou, *Nano Lett.*, 2010, **10**, 638.
- 21 J. Wu, A. Gross and H. Yang, *Nano Lett.*, 2011, **11**, 798.
- 22 C. Cui, L. Gan, M. Heggen, S. Rudi and P. Strasser, *Nat. Mater.*, 2013, **12**, 765.
- 23 L. Gan, C. Cui, M. Heggen, F. Dionigi, S. Rudi and P. Strasser, *Science*, 2014, **346**, 1502.
- 24 B. Han, C. E. Carlton, A. Kongkanand, R. S. Kukreja, B. R. Theobald, L. Gan, R. O'Malley, P. Strasser, F. T. Wagner and Y. Shao-Horn, *Energy Environ. Sci.*, 2015, **8**, 258.
- 25 K. A. Kuttiyiel, K. Sasaki, Y. Choi, D. Su, P. Liu and R. R. Adzic, *Nano Lett.*, 2012, **12**, 6266–6271.
- 26 Z. Zhang, G. Liu, X. Cui, B. Chen, Y. Zhu, Y. Gong, F. Saleem, S. Xi, Y. Du, A. Borgna, Z. Lai, Q. Zhang, B. Li, Y. Zong, Y. Han, L. Gu and H. Zhang, *Adv. Mater.*, 2018, **30**, 1801741.
- 27 N. Tian, Z. Y. Zhou, S. G. Sun, Y. Ding and Z. L. Wang, *Science*, 2007, **316**, 732.
- 28 Y. Ma, Q. Kuang, Z. Jiang, Z. Xie, R. Huang and L. Zheng, *Angew. Chem., Int. Ed.*, 2008, **47**, 8901.
- 29 L. Zhang, J. Zhang, Q. Kuang, S. Xie, Z. Jiang, Z. Xie and L. Zheng, *J. Am. Chem. Soc.*, 2011, **133**, 17114.
- 30 L. Zhang, Z. Xie and J. Gong, *Chem. Soc. Rev.*, 2016, **45**, 3916–3934.

- 31 L. Zhang, W. Niu and G. Xu, *Nano Today*, 2012, 7, 586.
- 32 Z. Quan, Y. Wang and J. Fang, *Acc. Chem. Res.*, 2013, 46, 191.
- 33 C. Zhu, D. Du, A. Eychmüller and Y. Lin, *Chem. Rev.*, 2015, 115, 8896.
- 34 Y. Kuroda, Y. Yamauchi and K. Kuroda, *Chem. Commun.*, 2010, 46, 1827.
- 35 H. Wang, M. Imura, Y. Nemoto, S.-E. Park and Y. Yamauchi, *Chem. – Asian J.*, 2012, 7, 802.
- 36 P. Karthika, H. Ataee-Esfahani, H. Wang, M. A. Francis, H. Abe, N. Rajalakshmi, K. S. Dhathathreyan, D. Arivuoli and Y. Yamauchi, *Chem. – Asian J.*, 2013, 8, 902.
- 37 G. S. Attard, J. M. Corker, C. G. Göltner, S. Henke and R. H. Templer, *Angew. Chem., Int. Ed.*, 1997, 36, 1315.
- 38 Y. Yamauchi, A. Sugiyama, R. Morimoto, A. Takai and K. Kuroda, *Angew. Chem., Int. Ed.*, 2008, 47, 5371.
- 39 H. Wang, L. Wang, T. Sato, Y. Sakamoto, S. Tominaka, K. Miyasaka, N. Miyamoto, Y. Nemoto, O. Terasaki and Y. Yamauchi, *Chem. Mater.*, 2012, 24, 1591.
- 40 C. Li, H. Wang and Y. Yamauchi, *Chem. – Eur. J.*, 2013, 19, 2242.
- 41 H. Wang, M. Imura, Y. Nemoto, L. Wang, H. Y. Jeong, T. Yokoshima, O. Terasaki and Y. Yamauchi, *Chem. – Eur. J.*, 2012, 18, 13142.
- 42 H. Wang and Y. Yamauchi, *Chem. – Asian J.*, 2012, 7, 2133.
- 43 Y. Yamauchi, A. Takai, T. Nagaura, S. Inoue and K. Kuroda, *J. Am. Chem. Soc.*, 2008, 130, 5426.
- 44 Y. Song, Y.-B. Jiang, H. Wang, D. A. Pena, Y. Qiu, J. E. Miller and J. A. Shelnett, *Nanotechnology*, 2006, 17, 1300.
- 45 Y. Xu and B. Zhang, *Chem. Soc. Rev.*, 2014, 43, 2439.
- 46 Y. Song, Y. Yang, C. J. Medforth, E. Pereira, A. K. Singh, H. Xu, Y. Jiang, C. J. Brinker, F. van Swol and J. A. Shelnett, *J. Am. Chem. Soc.*, 2004, 126, 635.
- 47 L. Wang and Y. Yamauchi, *J. Am. Chem. Soc.*, 2009, 131, 9152.
- 48 C. Kim, J.-G. Oh, Y.-T. Kim, H. Kim and H. Lee, *Electrochem. Commun.*, 2010, 12, 1596.
- 49 A. Mohanty, H. Garg and R. Jin, *Angew. Chem., Int. Ed.*, 2010, 49, 4962.
- 50 B. Lim, M. Jiang, P. H. C. Camargo, E. C. Cho, J. Tao, X. Lu, Y. Zhu and Y. Xia, *Science*, 2009, 324, 1302.
- 51 B. Lim, M. Jiang, T. Yu, P. H. C. Camargo and Y. Xia, *Nano Res.*, 2010, 3, 69.
- 52 Z. Peng and H. Yang, *J. Am. Chem. Soc.*, 2009, 131, 7542.
- 53 S. Guo, S. Dong and E. Wang, *ACS Nano*, 2010, 4, 547.
- 54 L. Wang, Y. Nemoto and Y. Yamauchi, *J. Am. Chem. Soc.*, 2011, 133, 9674.
- 55 N. T. Khi, J. Yoon, H. Baik, S. Lee, D. J. Ahn, S. J. Kwon and K. Lee, *CrystEngComm*, 2014, 16, 8312.
- 56 Z. Cai, C. Liu, G. Wu, X. Chen and X. Chen, *Electrochim. Acta*, 2014, 127, 377.
- 57 Y. Lou, C. Li, X. Gao, T. Bai, C. Chen, H. Huang, C. Liang, Z. Shi and S. Feng, *ACS Appl. Mater. Interfaces*, 2016, 8, 1614.
- 58 S. Guo, J. Li, S. Dong and E. Wang, *J. Phys. Chem. C*, 2010, 114, 15337.
- 59 W. Wang, D. Wang, X. Liu, Q. Peng and Y. Li, *Chem. Commun.*, 2013, 49, 2903.
- 60 Z. Cai, Y. Kuang, X. Qi, P. Wang, Y. Zhang, Z. Zhang and X. Sun, *J. Mater. Chem. A*, 2015, 3, 1182.
- 61 G. Chen, C. Xu, X. Huang, J. Ye, L. Gu, G. Li, Z. Tang, B. Wu, H. Yang, Z. Zhao, Z. Zhou, G. Fu and N. Zheng, *Nat. Mater.*, 2016, 15, 564.
- 62 M. E. Scofield, C. Koenigsmann, L. Wang, H. Liu and S. S. Wong, *Energy Environ. Sci.*, 2015, 8, 350.
- 63 B. Y. Xia, H. B. Wu, Y. Yan, X. W. Lou and X. Wang, *J. Am. Chem. Soc.*, 2013, 135, 9480.
- 64 Q. Xiao, M. Cai, M. P. Balogh, M. M. Tessema and Y. Lu, *Nano Res.*, 2012, 5, 145.
- 65 X. Teng, W.-Q. Han, W. Ku and M. Hucker, *Angew. Chem., Int. Ed.*, 2008, 47, 2055.
- 66 K. Jiang, D. Zhao, S. Guo, X. Zhang, X. Zhu, J. Guo, G. Lu and X. Huang, *Sci. Adv.*, 2017, 3, e1601705.
- 67 Z. Zhang, M. Li, Z. Wu and W. Li, *Nanotechnology*, 2011, 22, 015602.
- 68 S. Sun, G. Zhang, Y. Zhong, H. Liu, R. Li, X. Zhou and X. Sun, *Chem. Commun.*, 2009, 7048.
- 69 H. Yin, S. Zhao, K. Zhao, A. Muqsit, H. Tang, L. Chang, H. Zhao, Y. Gao and Z. Tang, *Nat. Commun.*, 2015, 6, 6430.
- 70 W. Lu, J. Ge, L. Tao, X. Cao, J. Dong and W. Qian, *Electrochim. Acta*, 2014, 130, 335.
- 71 S. Sun, G. Zhang, D. Geng, Y. Chen, R. Li, M. Cai and X. Sun, *Chem. – Eur. J.*, 2010, 16, 829.
- 72 S. Sun, F. Jaouen and J.-P. Dodelet, *Adv. Mater.*, 2008, 20, 3900.
- 73 X. Teng, M. Feyngenson, Q. Wang, J. He, W. Du, A. I. Frenkel, W. Han and M. Aronson, *Nano Lett.*, 2009, 9, 3177.
- 74 M. Li, Z. Zhao, T. Cheng, A. Fortunelli, C.-Y. Chen, R. Yu, Q. Zhang, L. Gu, B. V. Merinov, Z. Lin, E. Zhu, T. Yu, Q. Jia, J. Guo, L. Zhang, W. A. Goddard III, Y. Huang and X. Duan, *Science*, 2016, 354, 1414.
- 75 J. Zhang, Y. Mo, M. B. Vukmirovic, R. Klie, K. Sasaki and R. R. Adzic, *J. Phys. Chem. B*, 2004, 108, 10955.
- 76 J. X. Wang, H. Inada, L. Wu, Y. Zhu, Y. Choi, P. Liu, W.-P. Zhou and R. R. Adzic, *J. Am. Chem. Soc.*, 2009, 131, 17298.
- 77 K. Sasaki, H. Naohara, Y. Choi, Y. Cai, W.-F. Chen, P. Liu and R. R. Adzic, *Nat. Commun.*, 2012, 3, 1115.
- 78 H. Nan, X. Tian, J. Luo, D. Dang, R. Chen, L. Liu, X. Li, J. Zeng and S. Liao, *J. Mater. Chem. A*, 2016, 4, 847.
- 79 X. Tian, J. Luo, H. Nan, H. Zou, R. Chen, T. Shu, X. Li, Y. Li, H. Song, S. Liao and R. R. Adzic, *J. Am. Chem. Soc.*, 2016, 138, 1575.
- 80 E. Toyoda, R. Jinnouchi, T. Ohsuna, T. Hatanaka, T. Aizawa, S. Otani, Y. Kido and Y. Morimoto, *Angew. Chem., Int. Ed.*, 2013, 52, 4137.
- 81 S. Xie, S.-I. Choi, N. Lu, L. T. Roling, J. A. Herron, L. Zhang, J. Park, J. Wang, M. J. Kim, Z. Xie, M. Mavrikakis and Y. Xia, *Nano Lett.*, 2014, 14, 3570.
- 82 X. Xia, S. Xie, M. Liu, H.-C. Peng, N. Lu, J. Wang, M. J. Kim and Y. Xia, *Proc. Natl. Acad. Sci. U. S. A.*, 2013, 110, 6669.
- 83 S. Bai, C. Wang, M. Deng, M. Gong, Y. Bai, J. Jiang and Y. Xiong, *Angew. Chem., Int. Ed.*, 2014, 53, 12120.
- 84 S. Bai, L. Yang, C. Wang, Y. Lin, J. Lu, J. Jiang and Y. Xiong, *Angew. Chem., Int. Ed.*, 2015, 54, 14810.

- 85 V. R. Stamenkovic, B. Fowler, B. S. Mun, G. Wang, P. N. Ross, C. A. Lucas and N. M. Markovic, *Science*, 2007, **315**, 493.
- 86 J. Park, L. Zhang, S.-I. Choi, L. T. Roling, N. Lu, J. A. Herron, S. Xie, J. Wang, M. J. Kim, M. Mavrikakis and Y. Xia, *ACS Nano*, 2015, **9**, 2635.
- 87 X. Wang, M. Luo, H. Huang, M. Chi, J. Howe, Z. Xie and Y. Xia, *ChemNanoMat*, 2016, **2**, 1086.
- 88 T. Bian, H. Zhang, Y. Jiang, C. Jin, J. Wu, H. Yang and D. Yang, *Nano Lett.*, 2015, **15**, 7808.
- 89 X. Wang, S.-I. Choi, L. T. Roling, M. Luo, C. Ma, L. Zhang, M. Chi, J. Liu, Z. Xie, J. A. Herron, M. Mavrikakis and Y. Xia, *Nat. Commun.*, 2015, **6**, 7594.
- 90 J. Wu, L. Qi, H. You, A. Gross, J. Li and H. Yang, *J. Am. Chem. Soc.*, 2012, **134**, 11880.
- 91 X. Wang, M. Vara, M. Luo, H. Huang, A. Ruditskiy, J. Park, S. Bao, J. Liu, J. Howe, M. Chi, Z. Xie and Y. Xia, *J. Am. Chem. Soc.*, 2015, **137**, 15036.
- 92 J. Chen, J. M. McLellan, A. Siekkinen, Y. Xiong, Z.-Y. Li and Y. Xia, *J. Am. Chem. Soc.*, 2006, **128**, 14776.
- 93 J. Chen, B. Wiley, J. M. McLellan, Y. Xiong, Z.-Y. Li and Y. Xia, *Nano Lett.*, 2005, **5**, 2058.
- 94 R. Wu, Q.-C. Kong, C. Fu, S.-Q. Lai, C. Ye, J.-Y. Liu, Y. Chen and J.-Q. Hu, *RSC Adv.*, 2013, **3**, 12577.
- 95 J. W. Hong, S. W. Kang, B.-S. Choi, D. Kim, S. B. Lee and S. W. Han, *ACS Nano*, 2012, **6**, 2410.
- 96 L. Zhang, L. T. Roling, X. Wang, M. Vara, M. Chi, J. Liu, S.-I. Choi, J. Park, J. A. Herron, Z. Xie, M. Mavrikakis and Y. Xia, *Science*, 2015, **349**, 412.
- 97 X. Wang, L. Figueroa-Cosme, X. Yang, M. Luo, J. Liu, Z. Xie and Y. Xia, *Nano Lett.*, 2016, **16**, 1467.
- 98 D. S. He, D. He, J. Wang, Y. Lin, P. Yin, X. Hong, Y. Wu and Y. Li, *J. Am. Chem. Soc.*, 2016, **138**, 1494.
- 99 H.-J. Jang, S. Hong and S. Park, *J. Mater. Chem.*, 2012, **22**, 19792.
- 100 H.-J. Jang, S. Ham, J. A. I. Acapulco, Y. Song, S. Hong, K. L. Shuford and S. Park, *J. Am. Chem. Soc.*, 2014, **136**, 17674.
- 101 Z. Fang, Y. Wang, C. Liu, S. Chen, W. Sang, C. Wang and J. Zeng, *Small*, 2015, **11**, 2593.
- 102 Z. Niu, N. Becknell, Y. Yu, D. Kim, C. Chen, N. Kornienko, G. A. Somorjai and P. Yang, *Nat. Mater.*, 2016, **15**, 1188.
- 103 L. Han, H. Liu, P. Cui, Z. Peng, S. Zhang and J. Yang, *Sci. Rep.*, 2014, **4**, 6414.
- 104 C. Chen, Y. Kang, Z. Huo, Z. Zhu, W. Huang, H. L. Xin, J. D. Snyder, D. Li, J. A. Herron, M. Mavrikakis, M. Chi, K. L. More, Y. Li, N. M. Markovic, G. A. Somorjai, P. Yang and V. R. Stamenkovic, *Science*, 2014, **343**, 1339.
- 105 Y. Wu, D. Wang, G. Zhou, R. Yu, C. Chen and Y. Li, *J. Am. Chem. Soc.*, 2014, **136**, 11594.
- 106 A. Oh, H. Baik, D. S. Choi, J. Y. Cheon, B. Kim, H. Kim, S. J. Kwon, S. H. Joo, Y. Jung and K. Lee, *ACS Nano*, 2015, **9**, 2856.
- 107 B. Y. Xia, H. B. Wu, X. Wang and X. W. Lou, *J. Am. Chem. Soc.*, 2012, **134**, 13934.
- 108 F. Nosheen, Z. Zhang, J. Zhuang and X. Wang, *Nanoscale*, 2013, **5**, 3660.
- 109 Y. Jia, Y. Jiang, J. Zhang, L. Zhang, Q. Chen, Z. Xie and L. Zheng, *J. Am. Chem. Soc.*, 2014, **136**, 3748.
- 110 J. Ding, X. Zhu, L. Bu, J. Yao, J. Guo, S. Guo and X. Huang, *Chem. Commun.*, 2015, **51**, 9722.
- 111 S. Chen, H. Su, Y. Wang, W. Wu and J. Zeng, *Angew. Chem.*, 2015, **127**, 110.
- 112 B. Y. Xia, H. B. Wu, X. Wang and X. W. Lou, *Angew. Chem., Int. Ed.*, 2013, **52**, 12337.
- 113 Y. Wang, Y. Chen, C. Nan, L. Li, D. Wang, Q. Peng and Y. Li, *Nano Res.*, 2015, **8**, 140.
- 114 N. Becknell, Y. Kang, C. Chen, J. Resasco, N. Kornienko, J. Guo, N. M. Markovic, G. A. Somorjai, V. R. Stamenkovic and P. Yang, *J. Am. Chem. Soc.*, 2015, **137**, 15817.
- 115 A. Oh, Y. Jin Sa, H. Hwang, H. Baik, J. Kim, B. Kim, S. H. Joo and K. Lee, *Nanoscale*, 2016, **8**, 16379.
- 116 Z. Zhang, Z. Luo, B. Chen, C. Wei, J. Zhao, J. Chen, X. Zhang, Z. Lai, Z. Fan, C. Tan, M. Zhao, Q. Lu, B. Li, Y. Zong, C. Yan, G. Wang, Z. J. Xu and H. Zhang, *Adv. Mater.*, 2016, **28**, 8712.
- 117 M. Shao, A. Peles and K. Shoemaker, *Nano Lett.*, 2011, **11**, 3714.
- 118 M. Nesselberger, S. Ashton, J. C. Meier, I. Katsounaros, K. J. J. Mayrhofer and M. Arenz, *J. Am. Chem. Soc.*, 2011, **133**, 17428.
- 119 W. Sheng, S. Chen, E. Vescovo and Y. Shao-Horn, *J. Electrochem. Soc.*, 2012, **159**, B96.
- 120 H. A. Gasteiger, S. S. Kocha, B. Sompalli and F. T. Wagner, *Appl. Catal., B*, 2005, **56**, 9.
- 121 K. Kinoshita, *J. Electrochem. Soc.*, 1990, **137**, 845.
- 122 K. J. J. Mayrhofer, D. Strmcnik, B. B. Blizanac, V. Stamenkovic, M. Arenz and N. M. Markovic, *Electrochim. Acta*, 2008, **53**, 3181.
- 123 N. Cheng, Y. Shao, J. Liu and X. Sun, *Nano Energy*, 2016, **29**, 220.
- 124 X. Yang, A. Wang, B. Qiao, J. Li, J. Liu and T. Zhang, *Acc. Chem. Res.*, 2013, **46**, 1740.
- 125 B. Qiao, A. Wang, X. Yang, L. F. Allard, Z. Jiang, Y. Cui, J. Liu, J. Li and T. Zhang, *Nat. Chem.*, 2011, **3**, 634.
- 126 C. H. Choi, M. Kim, H. C. Kwon, S. J. Cho, S. Yun, H.-T. Kim, K. J. J. Mayrhofer, H. Kim and M. Choi, *Nat. Commun.*, 2016, **7**, 10922.
- 127 S. Sun, G. Zhang, N. Gauquelin, N. Chen, J. Zhou, S. Yang, W. Chen, X. Meng, D. Geng, M. Banis, R. Li, S. Ye, S. Knights, G. Botton, T.-K. Sham and X. Sun, *Sci. Rep.*, 2013, **3**, 1775.
- 128 N. Cheng, S. Stambula, D. Wang, M. Banis, J. Liu, A. Riese, B. Xiao, R. Li, T.-K. Sham, L. Liu, G. Botton and X. Sun, *Nat. Commun.*, 2016, **7**, 13638.
- 129 J. Jones, H. Xiong, A. T. DeLaRiva, E. J. Peterson, H. Pham, S. R. Challa, G. Qi, S. Oh, M. H. Wiebenga, X. I. P. Hernández, Y. Wang and A. K. Datye, *Science*, 2016, **353**, 150.
- 130 N. Cheng, M. Banis, J. Liu, A. Riese, X. Li, R. Li, S. Ye, S. Knights and X. Sun, *Adv. Mater.*, 2015, **27**, 277.
- 131 Y.-T. Kim, K. Ohshima, K. Higashimine, T. Uruga, M. Takata, H. Suematsu and T. Mitani, *Angew. Chem.*, 2006, **118**, 421.

- 132 U. Heiz, A. Sanchez, S. Abbet and W.-D. Schneider, *J. Am. Chem. Soc.*, 1999, **121**, 3214.
- 133 Y. Zhai, D. Pierre, R. Si, W. Deng, P. Ferrin, A. U. Nilekar, G. Peng, J. A. Herron, D. C. Bell, H. Saltsburg, M. Mavrikakis and M. Flytzani-Stephanopoulos, *Science*, 2010, **329**, 1633.
- 134 L. Lin, W. Zhou, R. Gao, S. Yao, X. Zhang, W. Xu, S. Zheng, Z. Jiang, Q. Yu, Y.-W. Li, C. Shi, X.-D. Wen and D. Ma, *Nature*, 2017, **544**, 80.
- 135 S. Yang, J. Kim, Y. J. Tak, A. Soon and H. Lee, *Angew. Chem., Int. Ed.*, 2016, **55**, 2058.
- 136 X. Li, W. Bi, L. Zhang, S. Tao, W. Chu, Q. Zhang, Y. Luo, C. Wu and Y. Xie, *Adv. Mater.*, 2016, **28**, 2427.
- 137 J. Liu, M. Jiao, L. Lu, H. M. Barkholtz, Y. Li, Y. Wang, L. Jiang, Z. Wu, D.-J. Liu, L. Zhuang, C. Ma, J. Zeng, B. Zhang, D. Su, P. Song, W. Xing, W. Xu, Y. Wang, Z. Jiang and G. Sun, *Nat. Commun.*, 2017, **8**, 15938.
- 138 J. Zhang, X. Wu, W.-C. Cheong, W. Chen, R. Lin, J. Li, L. Zheng, W. Yan, L. Gu, C. Chen, Q. Peng, D. Wang and Y. Li, *Nat. Commun.*, 2018, **9**, 1002.
- 139 J. Lin, A. Wang, B. Qiao, X. Liu, X. Yang, X. Wang, J. Liang, J. Li, J. Liu and T. Zhang, *J. Am. Chem. Soc.*, 2013, **135**, 15314.
- 140 J. Lin, B. Qiao, J. Li, Y. Huang, A. Wang, L. Li, W. Zhang, L. F. Allard, X. Wang and T. Zhang, *Angew. Chem., Int. Ed.*, 2012, **51**, 2920.
- 141 H. Yan, Y. Lin, H. Wu, W. Zhang, Z. Sun, H. Cheng, W. Liu, C. Wang, J. Li, X. Huang, T. Yao, J. Yang, S. Wei and J. Lu, *Nat. Commun.*, 2017, **8**, 1070.
- 142 H. Li, L. Wang, Y. Dai, Z. Pu, Z. Lao, Y. Chen, M. Wang, X. Zheng, J. Zhu, W. Zhang, R. Si, C. Ma and J. Zeng, *Nat. Nanotechnol.*, 2018, **13**, 411.
- 143 T. Li, J. Liu, Y. Song and F. Wang, *ACS Catal.*, 2018, **8**, 8450.
- 144 H. Wei, K. Huang, D. Wang, R. Zhang, B. Ge, J. Ma, B. Wen, S. Zhang, Q. Li, M. Lei, C. Zhang, J. Irawan, L.-M. Liu and H. Wu, *Nat. Commun.*, 2017, **8**, 1490.
- 145 J. D. Kistler, N. Chotigkrai, P. Xu, B. Enderle, P. Praserttham, C.-Y. Chen, N. D. Browning and B. C. Gates, *Angew. Chem., Int. Ed.*, 2014, **53**, 8904.
- 146 L. Liu, U. Díaz, R. Arenal, G. Agostini, P. Concepción and A. Corma, *Nat. Mater.*, 2016, **16**, 132.
- 147 S. Wei, A. Li, J.-C. Liu, Z. Li, W. Chen, Y. Gong, Q. Zhang, W.-C. Cheong, Y. Wang, L. Zheng, H. Xiao, C. Chen, D. Wang, Q. Peng, L. Gu, X. Han, J. Li and Y. Li, *Nat. Nanotechnol.*, 2018, **13**, 856.
- 148 Y. Chen, S. Ji, W. Sun, W. Chen, J. Dong, J. Wen, J. Zhang, Z. Li, L. Zheng, C. Chen, Q. Peng, D. Wang and Y. Li, *J. Am. Chem. Soc.*, 2018, **140**, 7407.
- 149 J. Liu, F. R. Lucci, M. Yang, S. Lee, M. D. Marcinkowski, A. J. Therrien, C. T. Williams, E. C. H. Sykes and M. Flytzani-Stephanopoulos, *J. Am. Chem. Soc.*, 2016, **138**, 6396.
- 150 F. R. Lucci, J. Liu, M. D. Marcinkowski, M. Yang, L. F. Allard, M. Flytzani-Stephanopoulos and E. C. H. Sykes, *Nat. Commun.*, 2017, **8**, 1070.
- 151 M. D. Marcinkowski, J. Liu, C. J. Murphy, M. L. Liriano, N. A. Wasio, F. R. Lucci, M. Flytzani-Stephanopoulos and E. C. H. Sykes, *ACS Catal.*, 2017, **7**, 41.
- 152 M. D. Marcinkowski, M. T. Darby, J. Liu, J. M. Wimble, F. R. Lucci, S. Lee, A. Michaelides, M. Flytzani-Stephanopoulos, M. Stamatakis and E. C. H. Sykes, *Nat. Chem.*, 2018, **10**, 325.
- 153 Y. Zhai, D. Pierre, R. Si, W. Deng, P. Ferrin, A. U. Nilekar, G. Peng, J. A. Herron, D. C. Bell, H. Saltsburg, M. Mavrikakis and M. Flytzani-Stephanopoulos, *Science*, 2010, **329**, 1633.
- 154 B. Zugic, S. Zhang, D. C. Bell, F. Tao and M. Flytzani-Stephanopoulos, *J. Am. Chem. Soc.*, 2014, **136**, 3238.
- 155 M. Yang, J. Liu, S. Lee, B. Zugic, J. Huang, L. F. Allard and M. Flytzani-Stephanopoulos, *J. Am. Chem. Soc.*, 2015, **137**, 3470.
- 156 Department of Energy, *Multi-Year Research, Development and Demonstration Plan*, <http://www.eere.energy.gov>, 2012.
- 157 S. Siahrostami, A. Verdager-Casadevall, M. Karamad, D. Deiana, P. Malacrida, B. Wickman, M. Escudero-Escribano, E. A. Paoli, R. Frydendal, T. W. Hansen, I. Chorkendorff, I. E. L. Stephens and J. Rossmeisl, *Nat. Mater.*, 2013, **12**, 1137.
- 158 S. Yang, Y. J. Tak, J. Kim, A. Soon and H. Lee, *ACS Catal.*, 2017, **7**, 1301.
- 159 B. D. McNichol, *J. Electroanal. Chem.*, 1981, **118**, 71.
- 160 P. C. K. Vesborg, B. Seger and I. Chorkendorf, *J. Phys. Chem. Lett.*, 2015, **6**, 951.
- 161 G. Niu, A. Ruditskiy, M. Vara and Y. Xia, *Chem. Soc. Rev.*, 2015, **44**, 5806.
- 162 K. S. Elvira, X. C. I. Solvas, R. C. R. Wootton and A. J. deMello, *Nat. Chem.*, 2013, **5**, 905.